Experimental Characterization of Long-Chain Polymer Drilling Fluids

by

Mitchell David Johnson

THESIS

Presented to the Faculty of

The University of Texas at Austin

in Partial Fulfillment

of the Requirements for Special Honors

for the Degree of

BACHELOR OF SCIENCE

THE UNIVERSITY OF TEXAS AT AUSTIN

May 2018

Experimental Characterization of Long-Chain Polymer Drilling Fluids

APPROVED BY

SUPERVISOR

Dr. Eric van Oort, Supervisor

Acknowledgements

I would like to sincerely thank my advisor, Dr. Eric van Oort, whose ideas, guidance, feedback, and resources made this work possible. Dr. van Oort introduced me to the joy of scientific research, a discovery which has changed the trajectory of my career and for which I will be forever grateful.

Dr. Ali Karimi provided invaluable direction and critical feedback which substantially improved the quality of this work. I am thankful for his patience and for his willingness to share his time and expertise despite my initial lack of experience in the field. I would like to thank Besmir Hoxha for his assistance in designing and troubleshooting experiments, and Tesse Smitherman for her unfailing dependability and valuable advice on professional etiquette.

I am thankful for Sercan Gul's endless patience and for the comradery he provided during many hours of testing and troubleshooting. Daryl Nygaard and Glen Baum provided incredibly competent and consistent support throughout the experimental process, and I would like to thank them for their selfless devotion to the success of their students and the Department of Petroleum Engineering.

Finally, I would like to thank my family, without whom I would have none of the endless opportunities that I have been blessed with at The University of Texas at Austin. Their incredible support, love and devotion have propelled me forward through many challenges over the years, and I do not tell them enough how much I appreciate them.

Experimental Characterization of Long-Chain Polymer Drilling Fluids

Mitchell David Johnson
The University of Texas at Austin, 2018

Supervisor: Dr. Eric van Oort

Sophisticated new drilling technologies such as managed pressure drilling (MPD) and dual gradient drilling (DGD) rely critically on accurate hydraulics modeling. Current fluid measurement and characterization technology performs well under a variety of conditions, but long-chain polymer additives have been shown to introduce significant complexity into the process of predicting frictional pressure losses in drilling operations. Considering the frequent use of long-chain polymer additives as both viscosifiers and friction reducers in drilling, completions and well intervention operations, this work seeks to further investigate the behavior of fluids containing these materials and propose improvements to existing measurement and pressure loss prediction methods.

A series of experiments was performed using a fully automated high temperature pipe viscometer to understand the effects of long chain polymer-based additives on fluid behavior in laminar, transitional and turbulent flow. Frictional pressure losses were measured in a cesium formate fluid viscosified with concentrations of xanthan gum up to 2.5 lb/bbl at temperatures

ranging from 100 – 230°F. Results were compared with widely used theoretical models for frictional pressure losses, showing significant discrepancy between current theory and empirical results.

In light of this discrepancy, a new method for determining frictional pressure losses in turbulent flow was proposed and evaluated. Direct measurement of pressure losses using a flow loop was shown to provide substantially improved pressure prediction in turbulent flow when compared to theoretical correlations commonly used in industry. A field-scale prototype was also developed to apply the pipe viscometer concept, providing the means to conduct future field trials of the technology. The field prototype's ability to characterize complex drilling fluid behavior in both laminar and turbulent flow shows significant promise for future applications in the drilling fluids domain.

Table of Contents

List of Figures

List of Tables

Chapter 1

Introduction

In the midst of dramatic technical change in many industries, the process of drilling an oil or gas well continues to involve many manual operations. Incidents like the 2010 Deepwater Horizon blowout, which caused 11 fatalities and cost BP over $60B, illustrate the need to improve safety, consistency, and efficiency in drilling operations. Automating the drilling process removes people from harm's way and reduces the potential for human error.

The research presented here focuses on automation of the fluid component of the drilling process. Drilling fluid, commonly known as mud, is an essential component in drilling operations. It has four main functions (Bommer, 2015b):

1. Remove cuttings from the well
2. Create hydrostatic pressure to prevent influx of fluids from the formation
3. Stop the wellbore from collapsing inward
4. Cool and lubricate the bit and drill string

The ability of drilling mud to perform these functions is dependent upon its rheological parameters, which must be characterized because the fluid composition changes throughout the drilling process. Drilling mud is a complex mixture of bentonite, polymers, thinners, barite, and other associated materials. The quantities of these additives are constantly in flux. The rheology of a drilling fluid affects the pressure loss that occurs

when it flows through the drill string and annulus, which in turn affects the bottom hole pressure, which is the effective pressure that the mud applies to the formation. Keeping this pressure within acceptable limits is essential, and sensors are rarely available at the bottom of the well for empirical measurement. As a result, the drilling industry relies heavily on modeling techniques to predict this bottom hole pressure. The rheological parameters of the mud are an essential input in the process. Chapter 2 of this thesis provides a theoretical overview of drilling fluid rheology and hydraulics modeling as they are currently implemented in industry.

Long-chain polymer additives are frequently used in drilling applications. Some of these additives are used as thickeners, increasing the viscosity of the fluid to improve hole cleaning and prevent barite sag. Others function as friction reducers, suppressing turbulence and reducing frictional pressure losses in turbulent flow. An extensive experimental study was performed using xanthan gum, a commonly used long-chain polymer thickening agent. Frictional pressure loss in laminar and turbulent flow was predicted using a commonly used industry model and compared with experimental results. Increasing xanthan concentration was shown to cause model predictions to deviate from experimentally measured pressures losses. Results of this study are described in Chapter 3.

On many rig setups the mud rheology is characterized as infrequently as once per day (Karimi Vajargah et al., 2016). In some situations, the lack of up-to-date mud data can cause problems that stall drilling operations, introduce extra costs to fix, and cause

significant safety concerns. Additionally, rotational viscometers measure rheology at far lower shear rates than the mud experiences downhole. They are incapable of measuring the mud in turbulent flow, an important consideration because mud flow is often turbulent inside the drill string and on occasions in annular spaces.

A new, automated method of measuring mud rheology based on the principle of a pipe viscometer was implemented to address these issues. This system is much simpler to automate than the industry standard rotational viscometer and provides the user with data on fluid behavior in both laminar and turbulent flow. Karimi Vajargah et al. (2016) used a laboratory prototype to provide proof of concept for the pipe viscometer technology. To test the technology in the field, a prototype mud monitoring system constructed by Shell Oil Company was modified to function as a pipe viscometer. Chapter 4 explains the development of the pipe viscometer concept and its application to the mud monitoring system prototype.

Chapter 5 concludes this thesis, connecting the previous sections and providing suggestions for future work in the domain of drilling fluid automation.

Chapter 2

Drilling Hydraulics

Minimum and maximum allowable bottom hole pressures are determined by the pore pressure – or mud pressure required for wellbore stability, whichever of the two is higher – and fracture pressure gradients of the formation, respectively. If the bottom hole pressure drops below the pore pressure, formation fluids such as oil or gas can flow in from the wellbore or the well can collapse. If the pressure exceeds the fracture pressure, the rock will fracture, creating space for the fluid to flow into and causing drilling fluid losses. Figure 2.1 illustrates the “drilling window”, or the range of allowable pressures between these two limits.

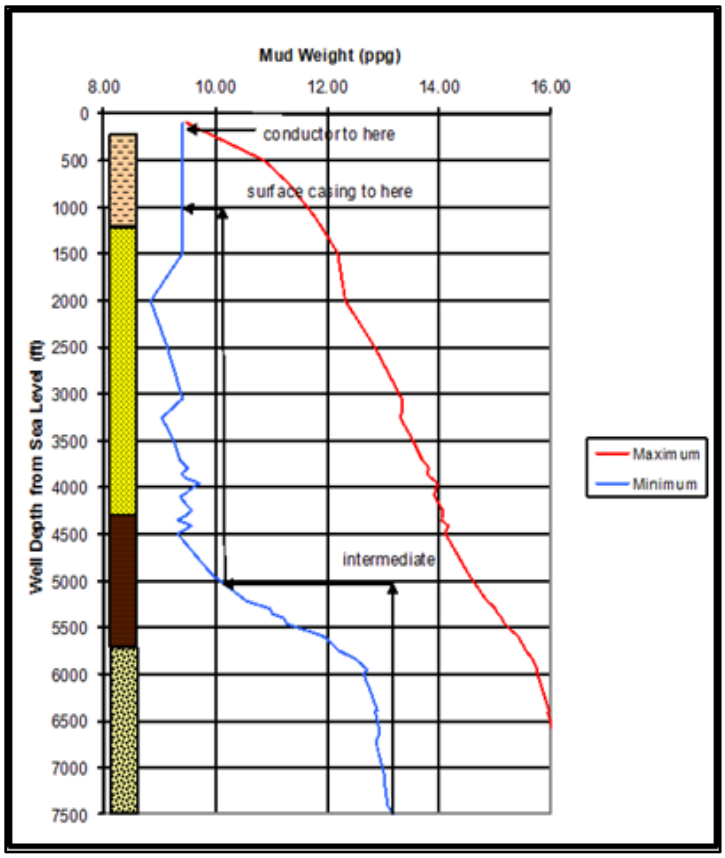

Figure 2.1 An example drilling window, showing the pressure as a function of the mud density required to create the equivalent pressure at a given depth (Bommer, 2015a).

To keep the bottom hole pressure inside the drilling window, drilling engineers must understand not only the hydrostatic pressure due to mud density, but also the dynamic pressure losses associated with mud flow through the drill pipe, bit, and annulus. These losses are related to the rheology of the fluid as well as its behavior in turbulent flow.

2.1 Drilling Fluid Rheology

2.1.1 Rheological Models

Rheology is the study of the deformation and flow of matter, particularly non-Newtonian fluids. Several rheological models are used to characterize drilling fluids, with the most commonly used described below.

Newtonian:

$$\tau = K\gamma \tag{2.1}$$

Power Law:

$$\tau = K\gamma^m \tag{2.2}$$

Bingham plastic:

$$\tau = \tau_y + K\gamma \tag{2.3}$$

Herschel Bulkley (1926), also known as Yield Power Law:

$$\tau = \tau_y + K\gamma^m \tag{2.4}$$

Figure 2.2 provides a graphical representation of the rheological models most commonly used for drilling fluids. The curves labeled “dilatant” and “pseudoplastic” represent Power Law fluids with m values greater and lesser than 1, respectively.

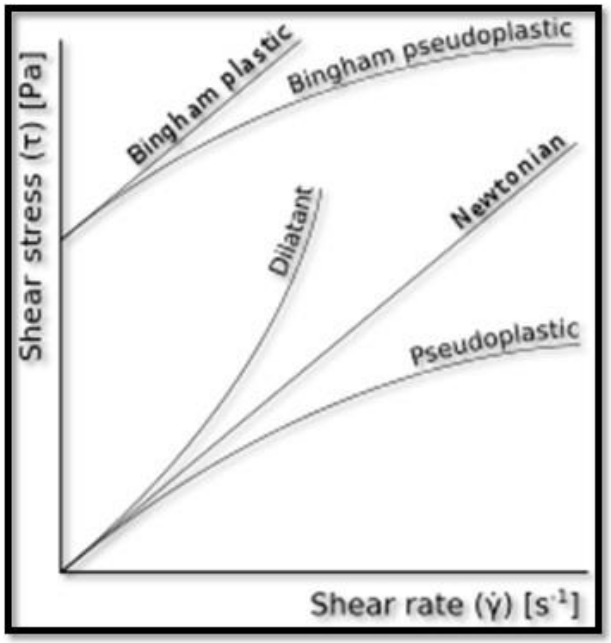

Figure 2.2: Graphical representation of the rheological models most commonly used for drilling fluids (Slashme, 2015).

The Yield Power Law (YPL) is widely used in drilling applications (Kelessidis et al., 2007 and 2011; Bailey and Peden, 2000; Hemphil et al., 1993; Mehrabi et al., 2012; Zamora, 2005). It is particularly versatile because it can be reduced to the simpler Bingham Plastic model or the Power Law model by setting m equal to 1 or τ_y equal to 0, respectively.

2.1.2 Determination of Rheological Parameters

A drilling fluid's rheological parameters must be determined to accurately predict its behavior downhole. This is done on drilling rigs by a rotational viscometer, shown in Figure 2.3.

Figure 2.3: Example of a rotational viscometer (Gardco, 2017).

This system measures the torque on a bob inside a cylinder which rotates at multiple speeds. A curve is fit to a graph of shear stress vs. shear rate, generating the parameters for one of the rheological models described above. Rotational viscometers measure rheology at far lower shear rates than mud experiences downhole. They are also incapable of measuring turbulent flow.

On many rig setups, mud rheology is characterized as infrequently as once per day (Karimi Vajargah et al., 2016). Any changes in the drilling mud that diminish performance should be caught and addressed quickly. However, with the current characterization techniques these changes might go unnoticed for 12 to 24 hours. In some situations, the lack of up-to-date mud data can cause problems that stall drilling operations, introduce

extra costs, and cause significant safety concerns. This research applies a concept called a pipe viscometer, described in further in Chapter 4, to improve these measurements.

2.2 Pressure Loss Prediction Methods

Once the rheological parameters of a drilling fluid have been determined, they are used to model the downhole behavior of the fluid. Frictional pressure losses inside the drill string and annulus are particularly important due to their effect on bottom hole pressure. Two approaches for pressure loss prediction are utilized here. The first applies the widely used Dodge and Metzner (1959) equation to predict the friction factor in turbulent flow, while the second approach uses real-time friction factor data by applying curve fitting techniques.

2.2.1 Industry Method

Frictional losses, otherwise known as major losses, occur due to viscous effects and turbulence in straight pipes (Munson et al., 2013). Prediction of frictional pressure losses requires the determination of a friction factor f for a given set of flow parameters. This friction factor is utilized in Equation 2.5 to calculate frictional pressure losses in any given pipe section.

$$\frac{dp}{dl} = \frac{2f\rho V^2}{D} \tag{2.5}$$

where V is the average fluid velocity, ρ is the fluid density, and D is the inner diameter of the pipe. This work uses the methodology presented by Kelessidis et al. (2011) to predict f in laminar, transitional, and turbulent flow. For laminar flow of YPL fluids, the friction factor is determined by first calculating the shear stress at the wall, τ_w, using Equation 2.6.

$$\frac{8V}{D} = \frac{(\tau_w - \tau_y)^{\frac{1+m}{m}}}{K^{\frac{1}{m}}\tau_w^3}\left(\frac{4m}{3m+1}\right)\left[\tau_w^2 + \frac{2m\tau_y\tau_w}{1+2m} + \frac{2m^2\tau_y^2}{(1+m)(1+2m)}\right] \tag{2.6}$$

where v is the fluid velocity, τ_y is the yield stress, K is the consistency index, and m is the fluid behavior index of the fluid being analyzed.

Once τ_w has been calculated using Equation 2.6 it can be used in Equation 2.7 to calculate the Reynolds number.

$$Re = \frac{8\rho V^2}{\tau_w} \tag{2.7}$$

The Reynolds number can then be utilized in Equation 2.8 to find the Fanning friction factor *f* for laminar flow.

$$f = \frac{16}{Re} \tag{2.8}$$

For turbulent flow, the correlation for non-Newtonian fluids developed by Dodge and Metzner (1959) provides a robust method for calculation of the friction factor. This correlation is represented below by Equation 2.9.

$$\frac{1}{\sqrt{f}} = \frac{4}{N^{0.75}} \log\left(Re \times f^{\left(1-\frac{N}{2}\right)}\right) - \frac{0.4}{N^{1.2}} \tag{2.9}$$

where Re is the Reynolds number, f is the Fanning friction factor and N is the generalized flow behavior index found in Equation 2.10.

$$\frac{1}{N} = \frac{(1-2m)\tau_w + 3m\tau_y}{m(\tau_w - \tau_y)} + \frac{2m(1+m)\left[(1+2m)\tau_w^2 + m\tau_y\tau_w\right]}{m(1+m)(1+2m)\tau_w^2 + 2m^2(1+m)\tau_w\tau_y + 2m^3\tau_y^2} \tag{2.10}$$

Equations 2.11 and 2.12 are used to determine whether flow is laminar or turbulent.

$$Re_1 = 3250 - 1150N \tag{2.11}$$

$$Re_2 = 4150 - 1150N \tag{2.12}$$

If the Reynolds number from Equation 2.7 is less than Re_1, the flow is assumed to be laminar and Equation 2.8 is used to predict the friction factor. If it is greater than Re_2, it is assumed to be turbulent and Equation 2.9 is used to predict the friction factor. Between these two thresholds a transition region exists where the friction factor is calculated by interpolating between the values calculated for fully laminar and fully turbulent flow. Once the friction factor is known, it is utilized in Equation 2.5 to predict frictional pressure losses. Kelessisids et al. (2011) presented this model and evaluated its accuracy using data from several experiments on water-based mud, demonstrating its success at predicting frictional pressure losses in the laminar and turbulent flow regimes.

2.2.2 Real-Time Measurement

A second approach presented here relies on automated real-time measurement of the friction factor. This procedure requires pressure vs. flow rate data and rheological parameters for the fluid under investigation. Pressure vs. flow rate data can be collected by a system identical to the experimental setup used in this study, with a pump, flow meter, and a section of straight pipe fitted with differential pressure transducers. Karimi Vajargah et al. (2016) demonstrated the viability of a method for using this same system to determine the rheological parameters of drilling fluids, meaning this entire process can be accomplished using a single testing apparatus.

Once the rheological parameters of the fluid have been determined and pressure vs. flow rate measurements have been obtained, the process for real-time determination of friction factor begins with the creation of a plot of friction factor vs. Reynolds number. Equation 2.6 is used to find the theoretical laminar values for τ_w for the given fluid velocity, and the corresponding Reynolds number is calculated with Equation 2.7. Rearranging Equation 2.5 to solve for f allows the friction factor to be determined for each data point. Once the friction factor vs. Reynolds number plot is generated for a particular fluid, a curve is fitted to the data and used to predict the friction factor at any Reynolds number within the domain of the data set.

Chapter 3

Experimental Investigation of Long-Chain Polymer Additives

3.1 Background

Long-chain polymers are commonly used as fluid additives in drilling, completions, and well intervention operations. Their tendency to modify rheological behavior and complicate modeling of fluids in turbulent flow is well known within the energy industry (Subramanian and Azar, 2000; Graham, 2004; API, 2010; Dosunmu and Shah, 2013; Karimi Vajargah et al., 2016).

Section 3.1.1 presents a brief background on the use of long-chain polymers as friction reducers, and Section 3.1.2 explains their use as viscosifiers. These two applications generated the impetus behind the experimental investigation described in this work.

3.1.1 Long-Chain Polymers as Friction Reducers

Toms (1948) conducted the first experiments proving the ability of small quantities of dissolved long-chain polymer molecules to substantially decrease frictional pressure losses in turbulent flow. The field of drag reduction has since garnered significant research interest, with applications ranging from ships (Hoyt, 1972) to pipelines (Graham, 2004). Experts in the field have generally agreed upon three essential characteristics for an

additive to function as a friction reducer: high molecular weight, polymer linearity, and solubility (Hoyt & Fabula, 1964; Gordon, 1970; Virk, 1975).

3.1.2 Long-Chain Polymers as Thickeners

Long-chain polymer additives are used as thickeners in many industries, including food processing, manufacturing of paint and other protective coatings, and in drilling and completion fluids (Glass et al., 1991). The rheology modifying capability of these materials comes from a combination of their high molecular weight, long-chain molecular structure, and their interactions with the surrounding fluid when placed in solution. A polymer additive's ability to thicken a solution is positively correlated with both molecular weight and concentration.

Xanthan gum, a product of the bacterium *Xanthomonas campestris*, is a commonly used long-chain polymer thickener. Its lack of toxicity makes it useful in a variety of industries, with applications ranging from cosmetics to enhanced oil recovery (García-Ochoa et al., 2000). In drilling and completions operations, xanthan gum is commonly used as a viscosifier to improve fluid loss, cuttings transport and barite sag (Khan et al., 2003; Navarrete et al., 2000). Its stability when subjected to high temperature, salinity, and mechanical shear make it particularly effective in well construction applications (Fischer et al., 2001; Salamone et al., 1992; Li et al., 1999; Beck et al., 1993).

It is interesting to note that the friction reducing agents described in Section 3.1.1 share the characteristics which make xanthan gum a successful thickener. The experimental

investigation presented in the remainder of this section will explore the crossover between these applications, wherein a long-chain polymer viscosifier like xanthan gum displays the characteristics of a friction reducing agent when the solution transitions to turbulent flow.

3.2 Experimental Setup

An experimental setup at The University of Texas at Austin was used to investigate frictional pressure drop in a wide variety of fluids. The experimental setup consists of a pump, Coriolis flow meter, two straight pipes of the same length and differing diameters, two differential pressure transducers, a heated reservoir, and a data acquisition and control system. Figure 3.1 provides a visual representation of the system layout.

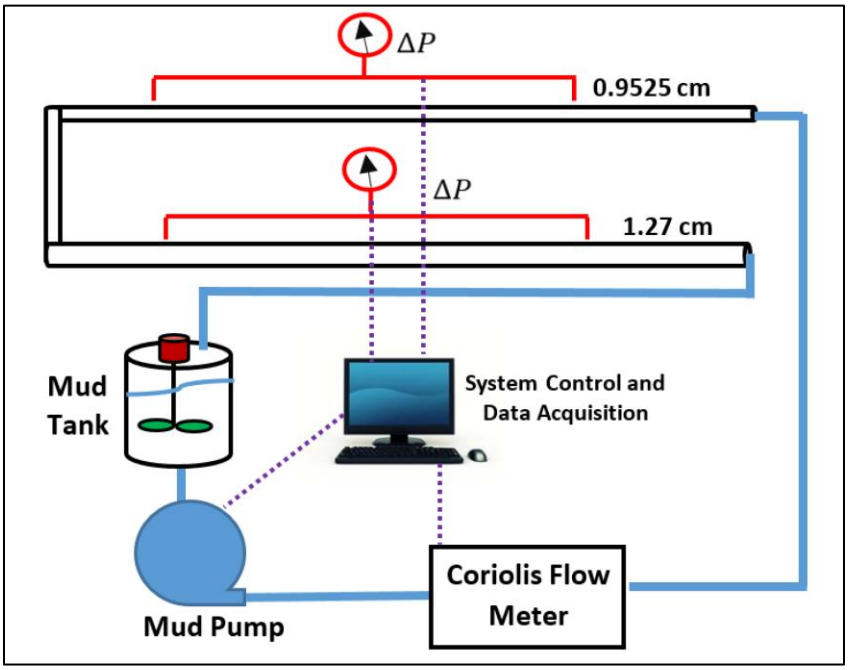

Figure 3.1: Diagram showing layout of experimental setup (Sullivan, 2016).

Kuzmyak (2014) constructed an initial prototype of this system, and Karimi Vajargah et al. (2016) made significant modifications to achieve its current capabilities. Sullivan (2016) provides a comprehensive description of all components included in the experimental setup and the process behind the system's development. The sections below describe modifications made for this work to improve reliability and provide the user with the capability to control the temperature at which the fluid is tested.

3.2.1 Piping

Karimi Vajargah et al. (2016) designed and constructed the pressure measurement system, which consists of two 316 series stainless steel tubes. The smaller tube, which has an outer diameter (OD) of 3/8 in (0.9525 cm), has an inner diameter (ID) of 0.305 in (0.7747 cm). The larger ½ in (1.270 cm) OD measurement tube has an ID of 0.430 in (1.0922 cm). One differential pressure sensor is connected to each tube by means tee fittings 10 ft (3.048 m) apart. Entrance and exit sections 4 ft (1.2192 m) in length were built into each tube to enable the flow to fully develop before the start of the measurement section. Empirical correlations from literature for non-Newtonian fluids were used to select this entrance and exit length (Collins and Schowalter, 1963). The total length of the measurement tubes is 18 ft (5.4864 m) including entrance and exit lengths.

When this work began, the piping system consisted of two stainless steel pressure measurement tubes connected by rubber hoses to a reservoir, flow meter and pump. These hoses simplified the process of setting up and rearranging the system, but they limited the

maximum operating pressure and temperature. Testing fluids at temperatures up to 230°F required replacing the rubber hoses from the initial design with high-temperature hoses designed for steam systems. Problems occurred with slippage and failure of the screw-on hose clamps while testing the upgraded hoses at high temperatures and pressures. These issues likely occurred due to differential thermal expansion between the clamp, pipe nipple, and hose. To remedy this issue, the entire system was upgraded to 1 in threaded 316 stainless steel piping. Insulation was installed on the reservoir and the piping components to minimize heat losses during testing.

3.2.2 Pump

Fluid is pressurized through the system by a model 2CL6-CSQ progressive cavity pump (PCP) from Continental Pump, selected and installed by Karimi Vajargah et al. (2016). PCPs are a type of positive displacement pump, which are useful in applications requiring a wide range of fluid viscosities and output pressures because these parameters have little effect on the flow rate (Petrowiki, 2018). Progressive cavity pumps have two primary components: a metallic rotor and an elastomeric stator (Cholet, 1997). They have a spiral design which creates many cavities between them when they are fitted together. As the rotor spins these cavities progress down the length of the pump, pressurizing the fluid in the process and forcing it out the end. The geometry of the pump creates even flow without pulsation, an important factor for obtaining consistent pressure measurements.

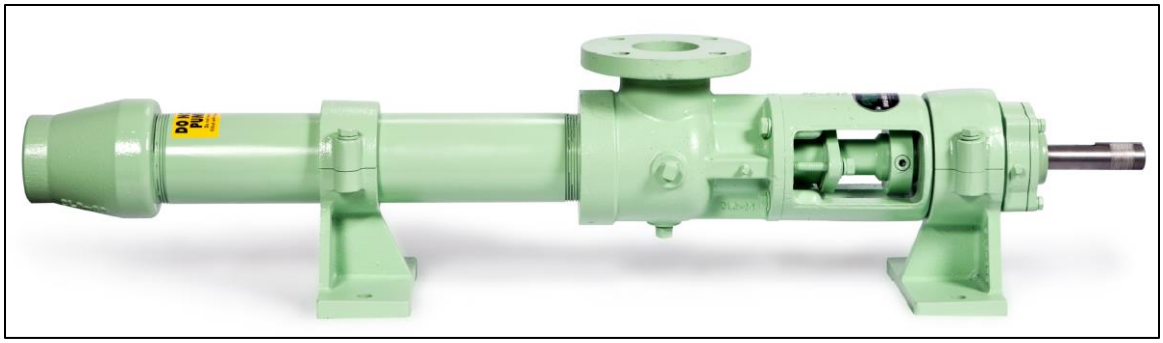

Figure 3.2: Image of a Continental Pump model 2CL6-CSQ (Continental Ultra Pumps, 2016).

The pump is driven by an electric motor, which is powered by alternating current from a variable frequency drive (VFD). By modulating the frequency of the alternating current from the VFD, the user can control the speed of the pump and the corresponding flow rate of the fluid.

3.2.3 Heating System

Controlling the temperature of the test fluid necessitated the development of a heater system for the experimental setup. Several potential system designs were evaluated, including a flow-through heater integrated into the piping system and a variety of heat sources attached to the tank. An immersion heater located inside the reservoir was determined to be the most cost-effective way to heat the fluid, so a 240V, 4500 Watt Inconel alloy heating element designed for use in home water heaters was installed in the tank. A type J thermocouple provides feedback to a Fuji Electric PXR4 temperature controller, which modulates power to the heater through a solid-state relay (SSR). This

heater system provided exceedingly reliable performance over the course of a month of continuous testing.

3.3 Experimental Results

Two phases of experiments were performed using the experimental setup described above. In the first phase, a variety of drilling fluids were tested and results were compared with the industry pressure loss prediction model described in Section 2.2.1 . In the second phase, the effect of a xanthan gum additive on frictional pressure loss was measured at concentrations from 0 to 2.5 lb/bbl and temperatures from 100 to 230°F.

3.3.1 Effect of Polymer Concentration on Industry Model Accuracy

An initial study was conducted on a variety of fluids to evaluate the accuracy of the model described in Section 2.2.1 . The five drilling fluids used in this study are described below, and the full composition of muds A and B is described in Table 3.1:

Mud A: water-based bentonite clay suspension, prepared in the lab with zero polymer content.

Mud B: water-based mud prepared in the lab with added polymers but no bentonite.

Mud C: water-based mud prepared in the field with proprietary formulation containing long-chain polymers.

Mud D: synthetic-based drilling fluid prepared in the field with proprietary formulation.

Mud E, E*, E:** water-based cesium/potassium formate brine with xanthan polymer added. Three different polymer concentrations were used (0.25 lb/bbl, 0.5 lb/bbl and 1.0 lb/bbl) to investigate the effect of polymer concentrations.

Table 3.1: Compositions of muds A and B.

Component	**Mud A**	**Mud B**
	Concentration (lb/bbl or gr/350 cc)	Concentration (lb/bbl or gr/350 cc)
Water	322.14	328.61
Bentonite	9.17	0
Xanvis	0	0.33
PAC R	0	0.67
Barite	10.36	12.06
Drilling cuttings	8.33	8.33

An OFITE 900 rotational viscometer was used to obtain the rheological parameters in accordance with a yield-power-law (YPL) rheological model. These parameters are catalogued in Table 3.2.

Table 3.2: YPL rheological properties (yield stress, τ_y, consistency index, K, and flow behavior index, m) and density for each fluid.

Fluid	$\boldsymbol{\tau_y}$ $\boldsymbol{(pa)}$	$\boldsymbol{K}$ $\boldsymbol{(Pa.s^m)}$	$\boldsymbol{m}$	Specific Gravity
Mud A	3.244	0.1109	0.7506	1.14
Mud B	2.139	0.5992	0.4679	1.12
Mud C	0	0.4079	0.5383	1.26
Mud D	0.9512	0.0318	0.9611	1.186
Mud E	0.7919	0.286	0.6526	1.87
Mud E*	0.5591	0.05246	0.8202	1.87
Mud E**	0.0195	0.03917	0.8191	1.87

Mud A, a bentonite clay mud with no polymer content, was measured at flow rates between 0.92 and 7.39 gpm. These flow rates corresponded to Reynolds numbers between 470 and 7200. Figure 3.3 shows predicted and measured pressure vs. flow rate values for Mud A, demonstrating excellent agreement between measured values and model predictions in both the laminar and turbulent flow regimes.

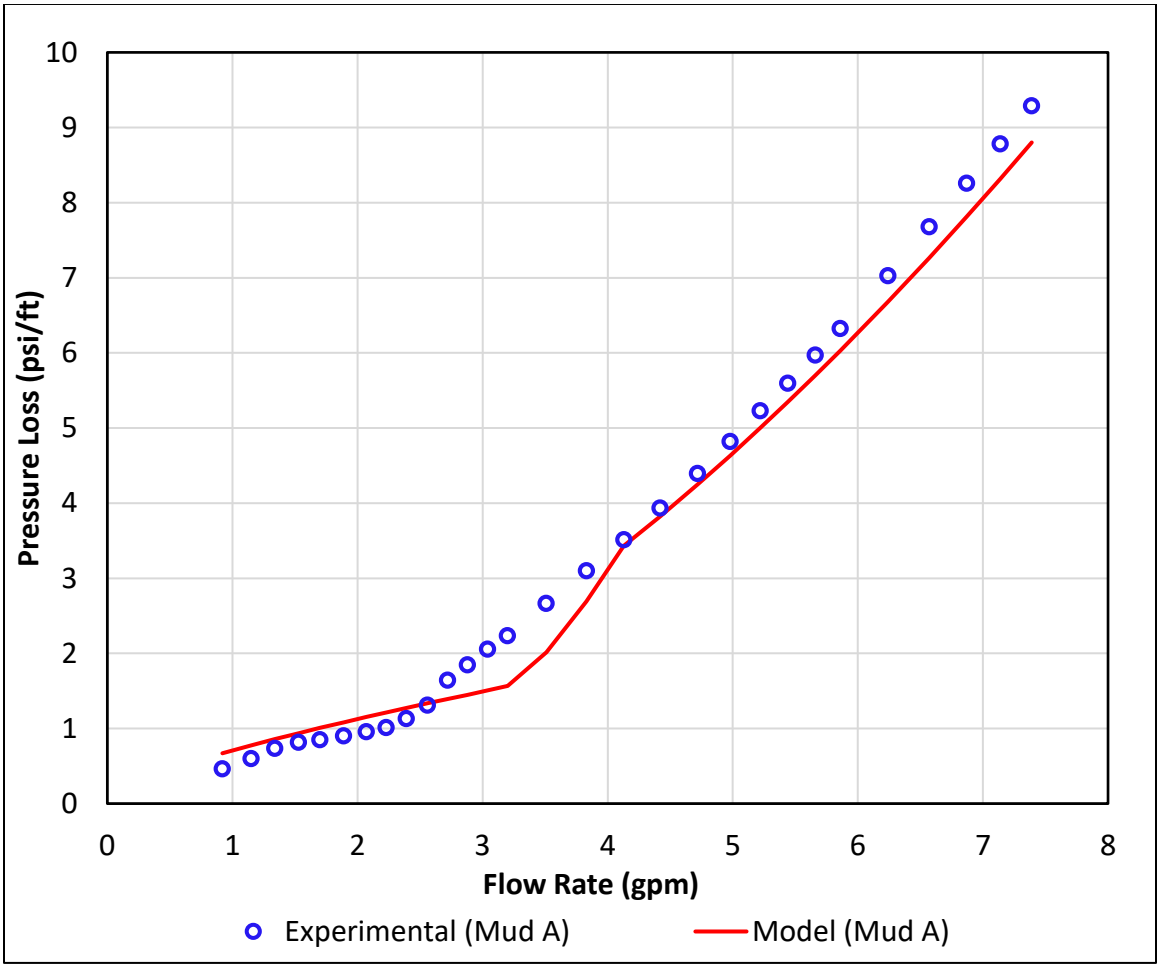

Figure 3.3: Comparison between values obtained from the experimental data and the model for Mud A (bentonite clay mud).

Figure 3.4 shows predicted and measured pressure vs. flow rate values for Mud B, which was tested at flow rates between 0.95 and 10.73 gpm. Reynolds numbers at these flow rates ranged from 640 to 29,500. Excellent agreement was observed between model predictions and experimental results in the laminar flow regime, but a major discrepancy emerged once the fluid transitioned to turbulence at approximately 2.5 gpm. Note that Mud B included substantial polymer content.

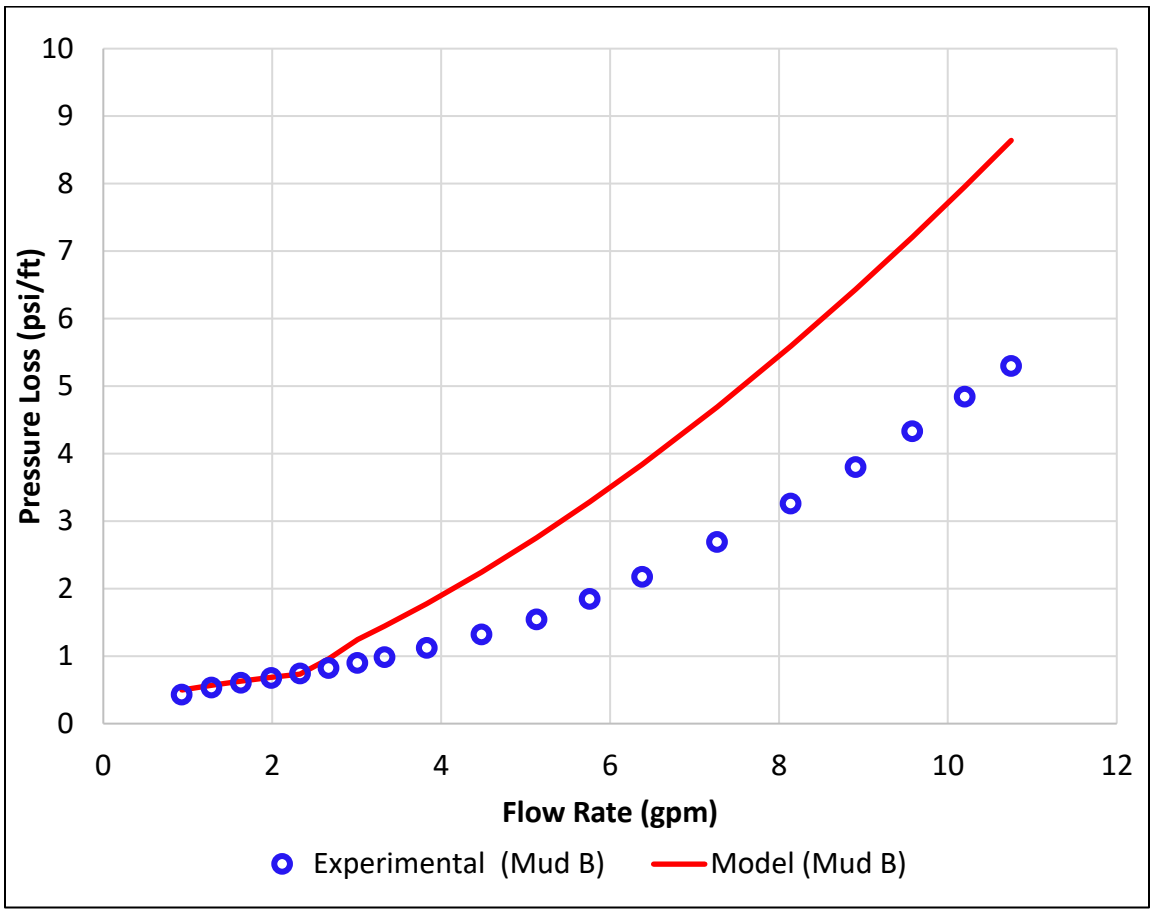

Figure 3.4: Comparison between values obtained from the experimental data and model for Mud B (polymer-based mud).

Mud C, which also contained polymers, was tested at flow rates ranging from 0.88 to 7.98 gpm. Reynolds numbers ranged from 700 and 17000. Figure 3.5 shows predicted and measured pressure vs. flow rate values for Mud C. The trend is similar to that of Mud B, with excellent agreement between predicted and experimental results in the laminar flow regime but a growing discrepancy appearing after the model's predicted transition to turbulence.

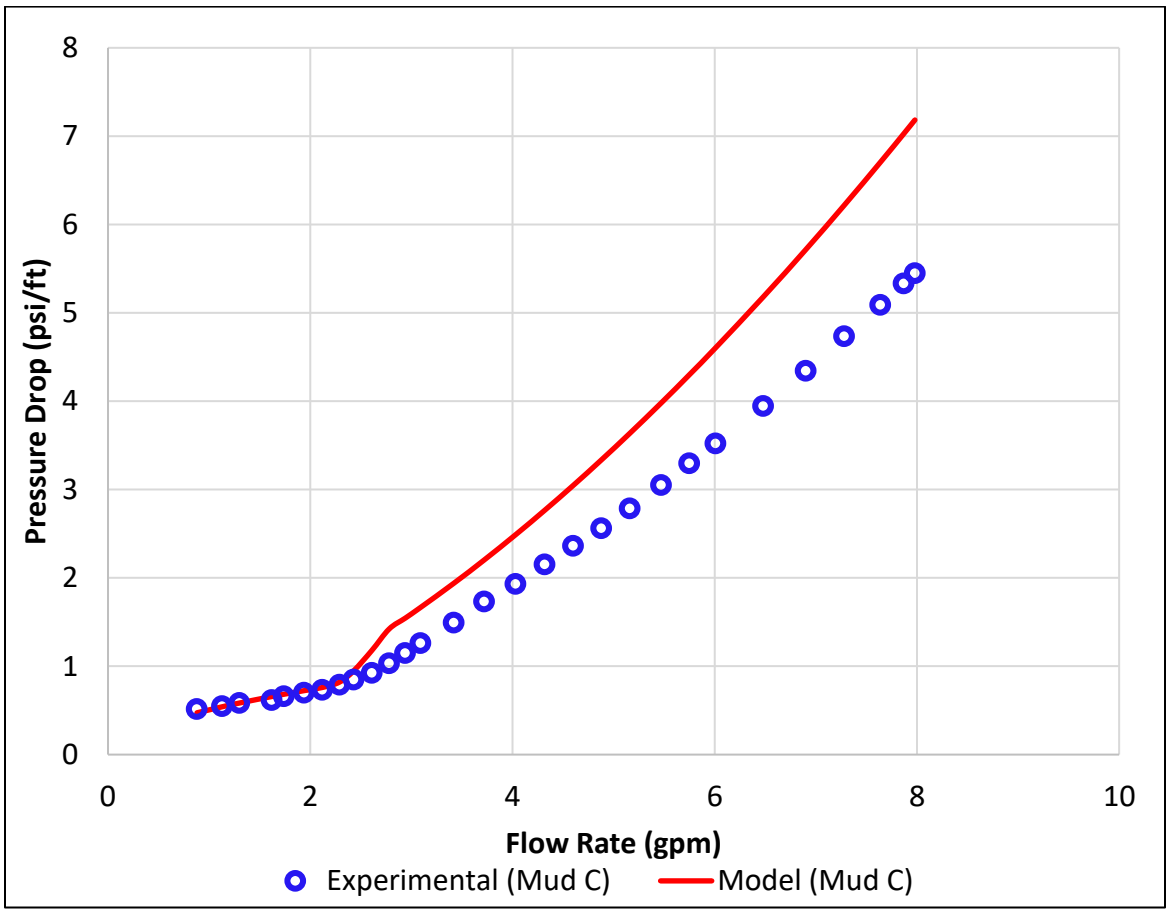

Figure 3.5: Comparison between values obtained from the experimental data and model for Mud C (polymer-based mud used in the field).

Mud D, a synthetic-based mud mixed in the field with a proprietary formulation, was tested at lower flow rates than the other muds due to system limitations. Flow rates ranged from 1.29 to 6.67 gpm, resulting in Reynolds numbers from approximately 600 to 3600. Figure 3.6 shows pressure vs. flow rate data for Mud D. Results showed strong agreement between predicted and measured pressure loss values, except for a moderate discrepancy in the transition region.

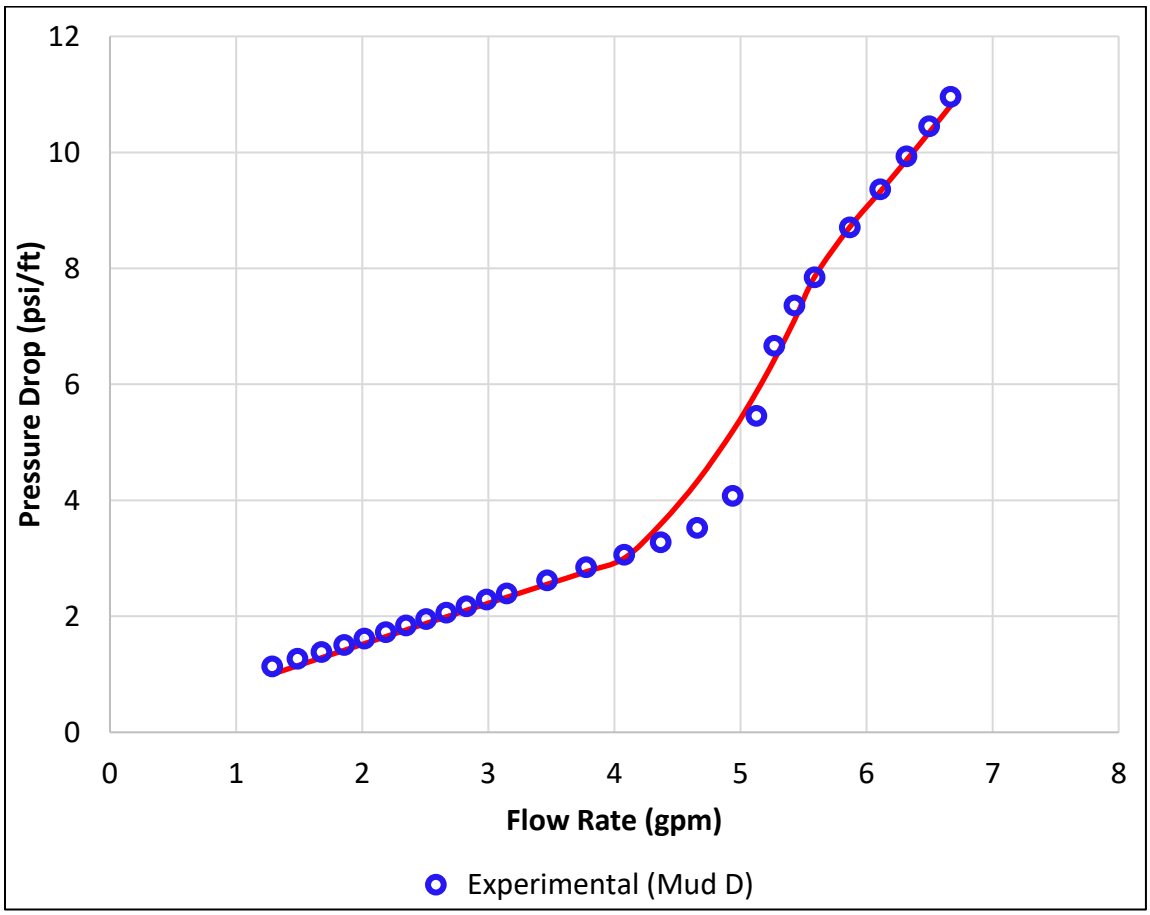

Figure 3.6: Comparison between values obtained from the experimental data and model for Mud D (synthetic-based mud used in the field).

The strong correlation between the pressure loss predictions and experimental data from Mud A and Mud D show that the model predictions are useful for a variety of fluids. However, both Mud B and Mud C, which contained long-chain polymers, experienced a substantial degradation in model accuracy in the turbulent flow regime. This insight warranted further investigation to better understand the friction reducing effects of these long-chain polymers. A concentration study was performed on Mud E, beginning with a xanthan concentration of 1 lb/bbl before successive dilution to 0.5 lb/bbl (Mud E*) and 0.25 lb/bbl (Mud E**).

Mud E, a water-based cesium/potassium formate brine containing 1 lb/bbl of xanthan polymer, was tested at flow rates ranging from 0.92 to 6.82 gpm. Reynolds numbers for these flow rates ranged from 660 to 10,100. Figure 3.7 shows predicted and measured pressure vs. flow rate data for Mud E. In turbulent flow a major discrepancy was observed between the model and the experimental results, while model predictions remained largely accurate in laminar flow. This trend is similar to results from the other high polymer content fluids discussed above.

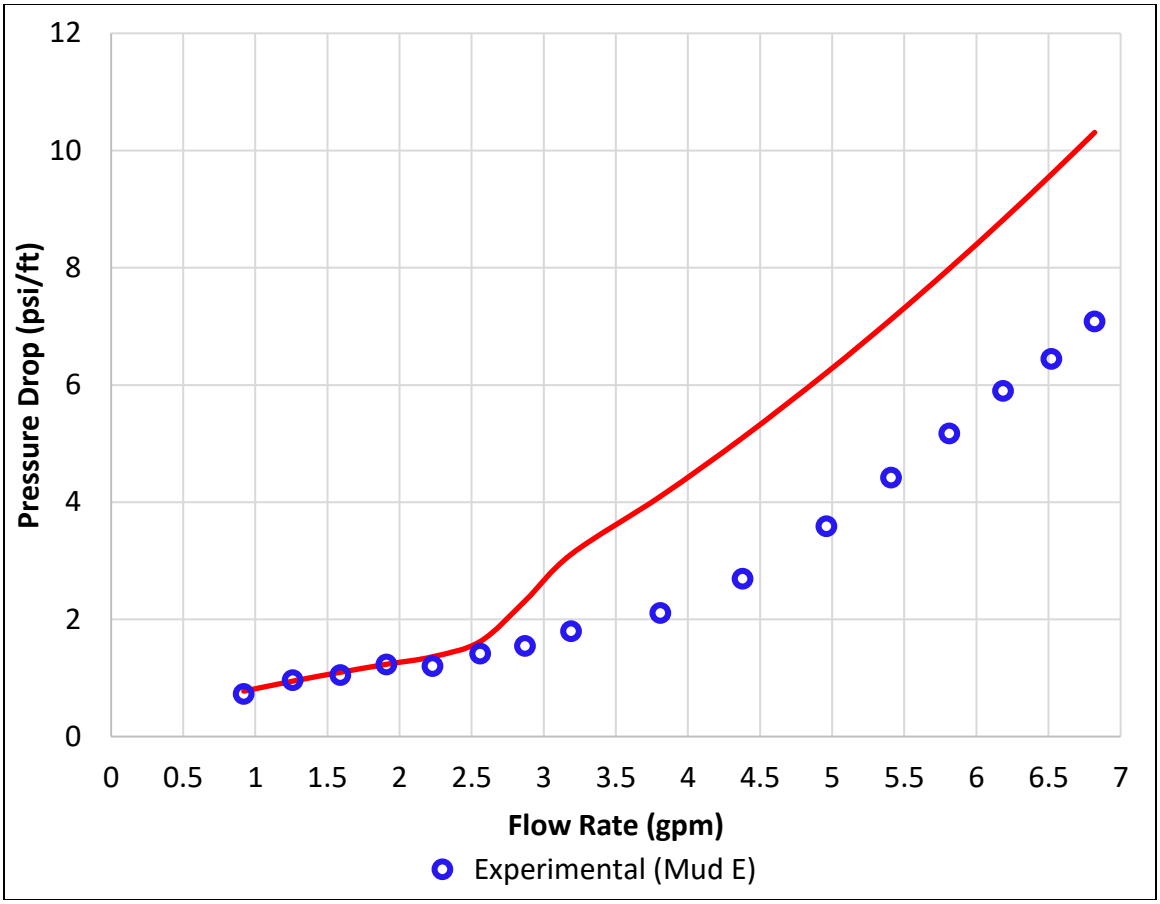

Figure 3.7: Comparison between values obtained from the experimental data and model for Mud E (Cesium formate mud with xanthan gum).

Mud E*, created by diluting Mud E to a xanthan concentration of 0.5 lb/bbl, was tested at flow rates between 0.95 and 6.01 gpm. Reynolds numbers ranged between 1,170 and 10,680. Figure 3.8 displays predicted and measured pressure vs. flow rate values for Mud E*. Agreement between the model and the experimental data improved in turbulent flow, with a smaller margin of error visible when compared to Mud E.

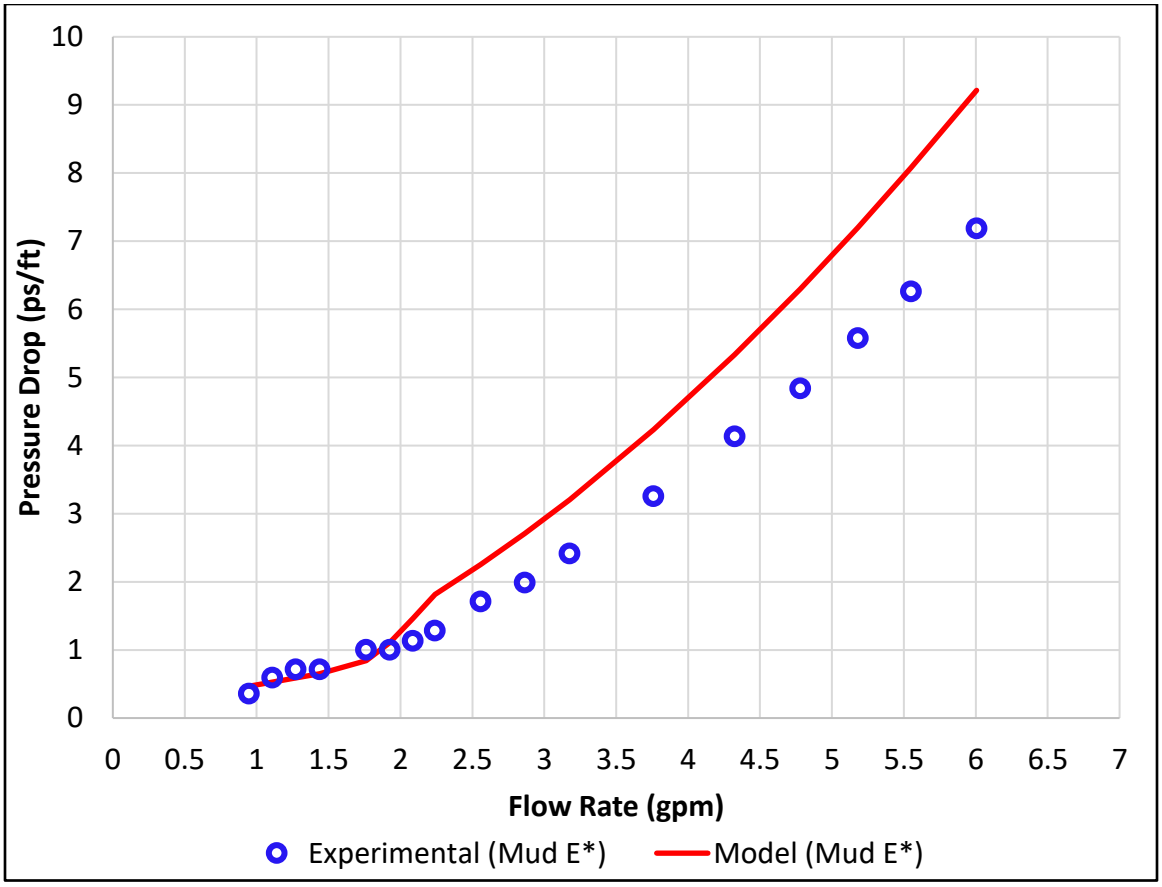

Figure 3.8: Comparison between values obtained from the experimental data and model for Mud E*.

Figure 3.9 shows pressure vs. flow rate data from Mud E**, created by diluting Mud E to a xanthan concentration of 0.25 lb/bbl. Flow rates ranged from 0.57 and 5.57 gpm during this test, resulting in Reynolds numbers between 1,330 and 13,350. Agreement between model predictions and experimental data is quite excellent in both the laminar and turbulent flow regimes, rendering the effects of polymer content on model accuracy unnoticeable at this xanthan concentration.

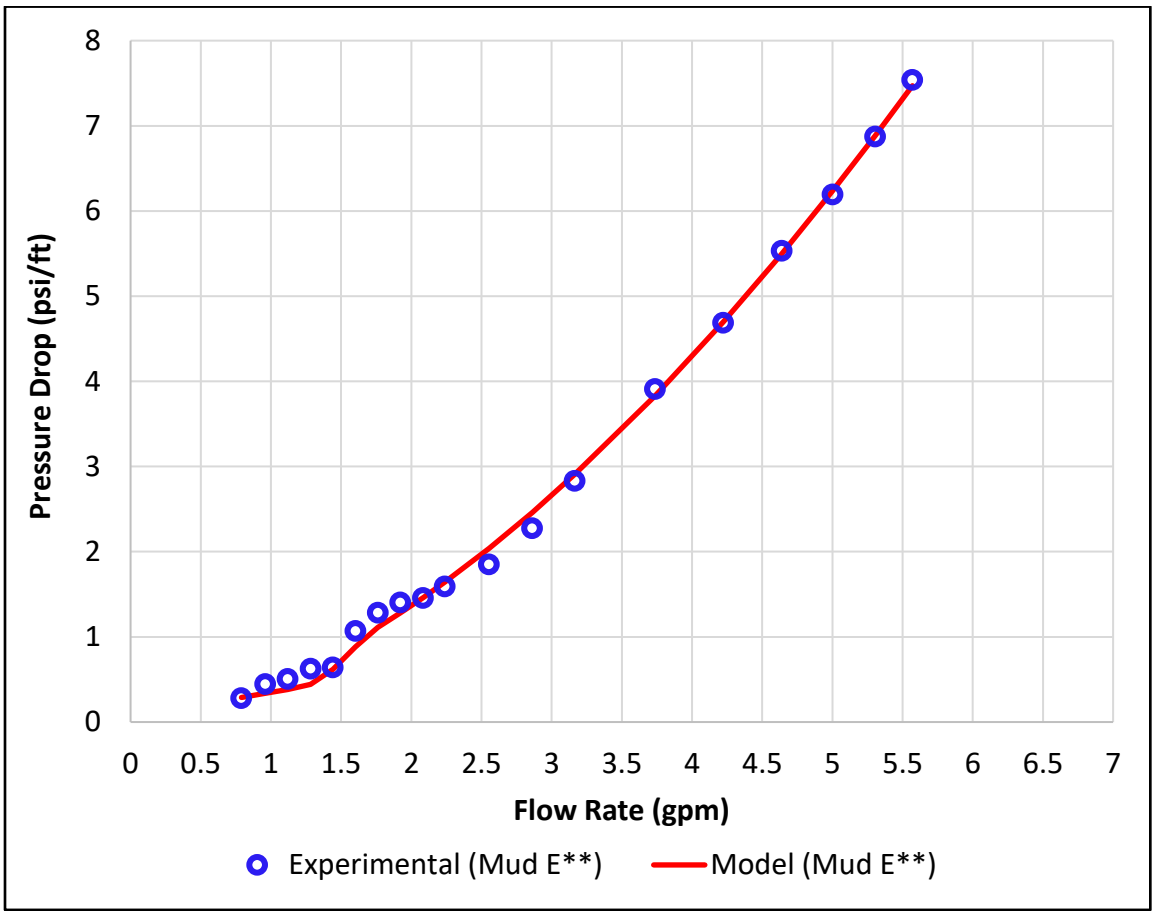

Figure 3.9: Comparison between values obtained from the experimental data and model for Mud E**.

The preceding results show that xanthan polymer has a significant effect on the accuracy of Dodge and Metzner's (1959) correlation for frictional pressure loss in turbulent flow of non-Newtonian fluids. The complex behavior of fluids containing xanthan polymer leads to two important conclusions.

First, accurately predicting the behavior of drilling fluids downhole using models and correlations from literature is a complicated endeavor that lacks precision. Second, drilling fluids containing long-chain polymer additives behave in particularly unique and unexpected ways when analyzed in both laminar and turbulent flow. In some scenarios this is no surprise; a friction reducing additive would be expected to lower pressure losses in turbulent flow, and a viscosifier to increase pressure losses in laminar flow. In this case, however, an additive which is traditionally used as a viscosifier has been shown to also behave as a friction reducer when the fluid transitions to turbulence. This unexpected result further complicates the prediction of frictional pressure losses, which is concerning considering the prevalence of long-chain polymer additives in drilling and completions operations. These conclusions warranted a more in-depth experimental evaluation, described in the following sections.

3.3.2 Effect of Polymer Concentration on Frictional Pressure Loss

The previous section discussed anomalies in pressure loss predictions for high polymer content fluids. To further investigate these anomalies, this section presents a more comprehensive polymer concentration study using xanthan gum. Cesium formate brine

was used as the base fluid for this study and tests were performed with xanthan additive concentrations from 0 to 2.5 lb/bbl. Pressure loss vs. flow rate data from all concentrations tested at 100°F are shown in Figure 3.10.

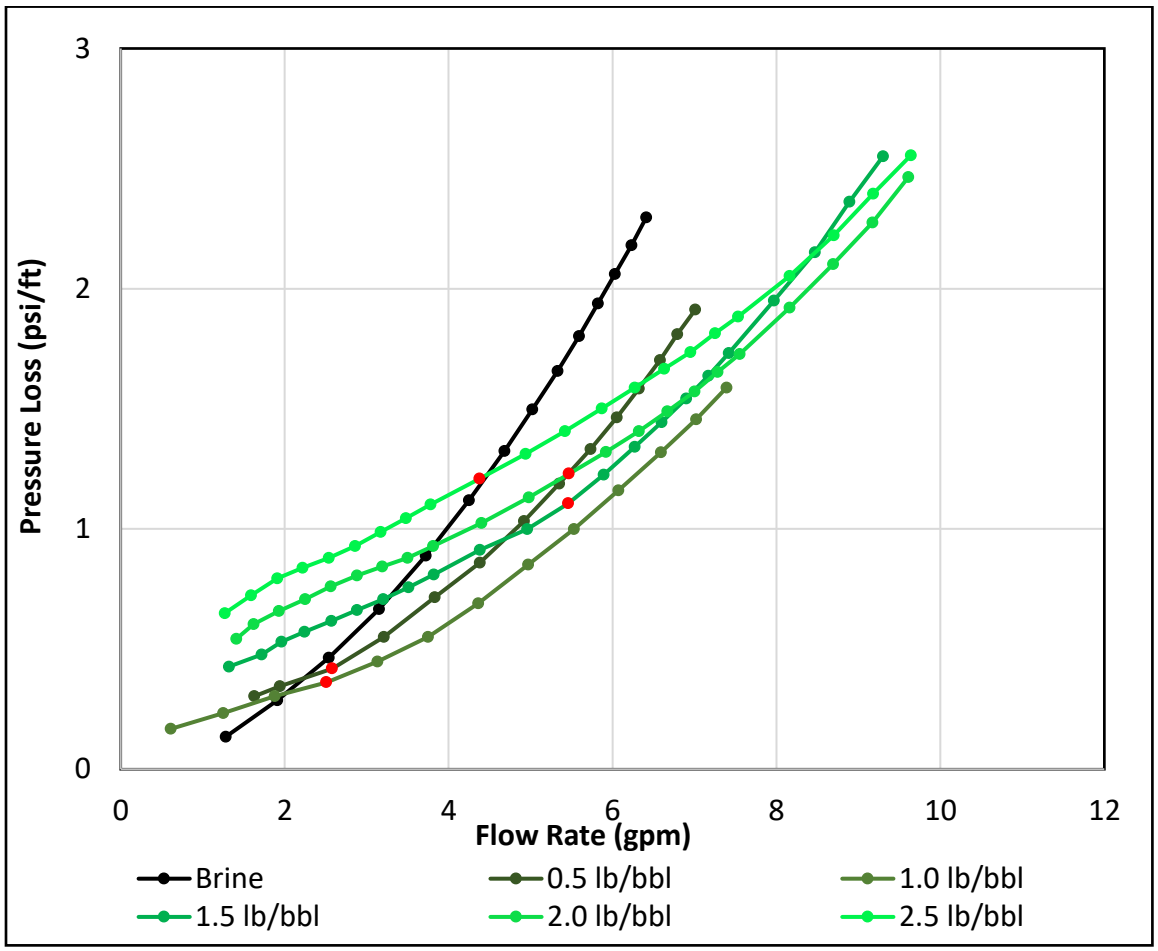

Figure 3.10: Experimental data from cesium formate brine in a ½ in tube at 100°F with xanthan concentrations from 0 to 2.5 lb/bbl. Red dots represent the last laminar data point before the flow begins to transition to turbulence.

To assist in the interpretation of these results, red dots mark the data points where turbulent flow is predicted to begin for each fluid. This transition point was estimated by

creating a plot of friction factor vs. flow rate as shown in Figure 3.11**.** A straight line was added to this figure following the slope of the laminar flow region. The first data point deviating from this trend was assumed to indicate a transition to turbulence.

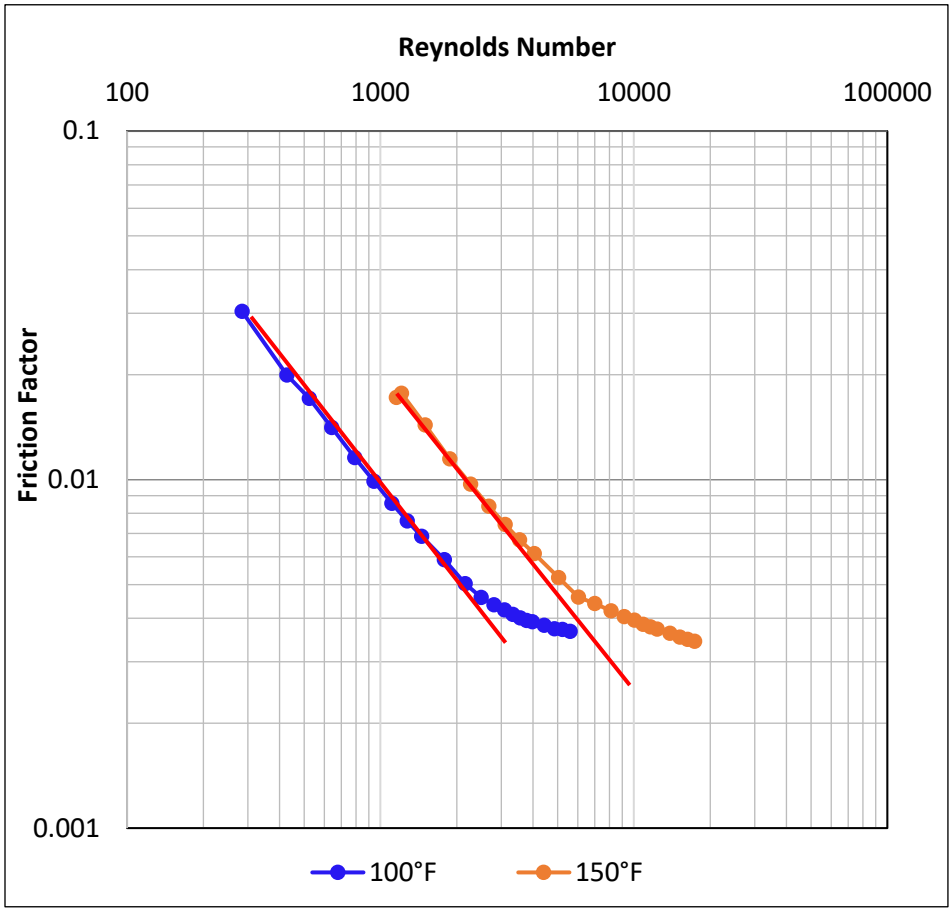

Figure 3.11: Chart of friction factor vs. Reynolds number for cesium formate brine containing 1.5 lb/bbl xanthan at two temperatures. The red line was assumed to represent the laminar portion of the test data.

Figure 3.10 shows an intriguing contrast between the laminar and turbulent flow regime. In laminar flow, higher xanthan concentrations resulted in increased frictional

pressure losses, with the highest polymer content fluid showing frictional pressure losses greater than 3x those of the base brine at 1.3 gpm.

In turbulent flow, however, the trend reversed. By the time flow reached 5 gpm, the brine had the highest frictional pressure loss of all fluids tested, and the disparity continued to grow at higher flow rates. Although equipment limitations prevented testing lower xanthan concentrations at flow rates up to 10 gpm, the slope of the curves shows a strong likelihood that the order of data series on the graph would completely invert (i.e. highest xanthan concentrations exhibiting lowest frictional pressure loss) at higher flow rates.

Tests conducted at 150°F show that this inversion does indeed occur at higher Reynolds numbers. Figure 3.12 shows pressure loss vs. flow rate for all polymer concentrations tested at 150°F in the ½ in OD tube. Trends in the data series appear similar to those observed at 100°F, but with an earlier inversion point between the laminar and turbulent pressure trends. This result is to be expected due to the decreased viscosity of all fluids at increased temperature, causing the flow to transition to turbulence at lower flow rates.

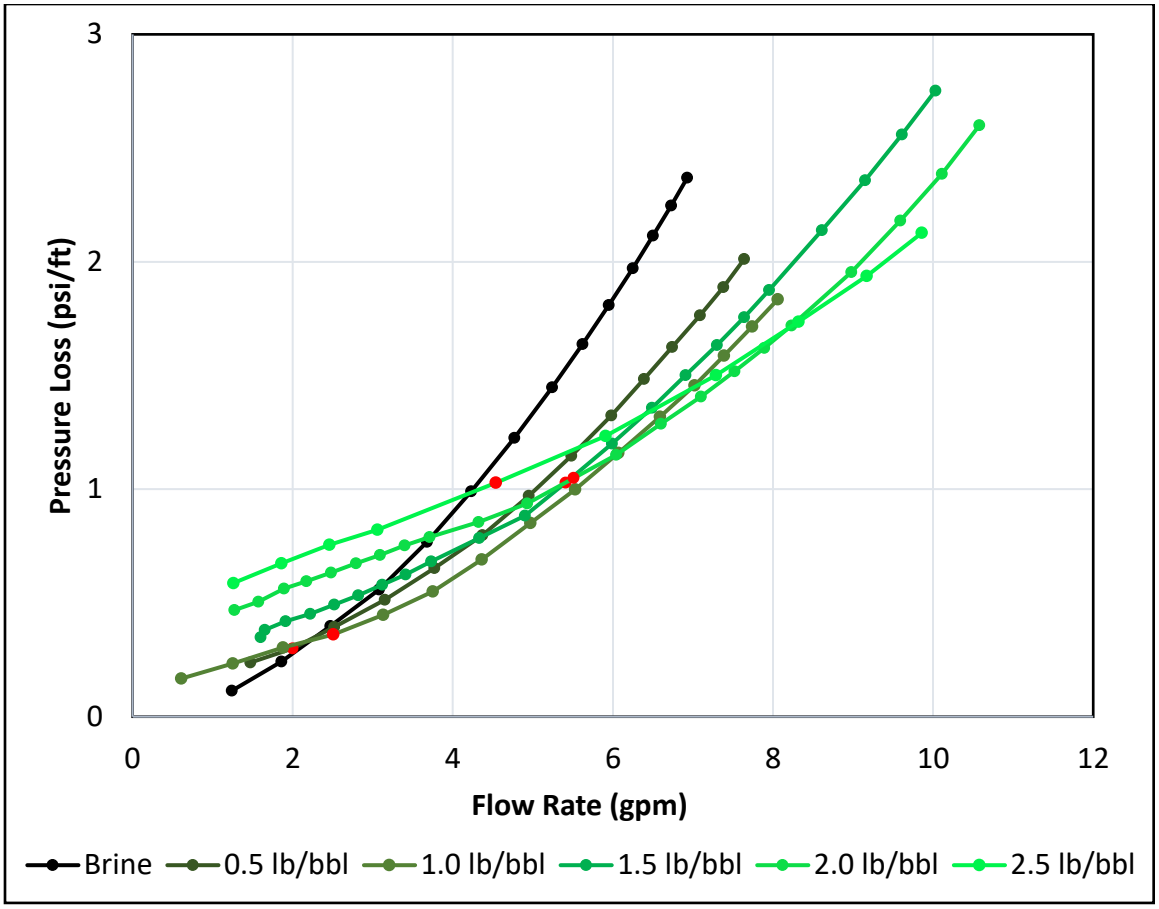

Figure 3.12: Experimental data from cesium formate brine in a ½ in OD tube at 150°F with xanthan concentrations from 0 to 2.5 lb/bbl. Red dots represent the last laminar data point before the flow begins to transition to turbulence.

Flow in the 3/8" tube at 150°F is turbulent for almost the entire range of flow rates and xanthan concentrations tested. Graphing the friction factor vs. Reynolds number allows for a more thorough examination of the turbulent pressure trend, which shows a decreasing friction factor with increasing xanthan concentration. Figure 3.13 shows friction factor vs. Reynolds numbers for all fluid concentrations at 150°F in the 3/8 in OD tube. Note that the gap in friction factor between the brine (no xanthan) and the fluid with 0.5 lb/bbl xanthan

is significantly larger than the gaps between the fluids of higher polymer concentrations. Each 0.5 lb/bbl increase in polymer concentration led to a successively smaller reduction in pressure loss, implying that the drag reducing effect of further xanthan additions diminishes beyond a certain point.

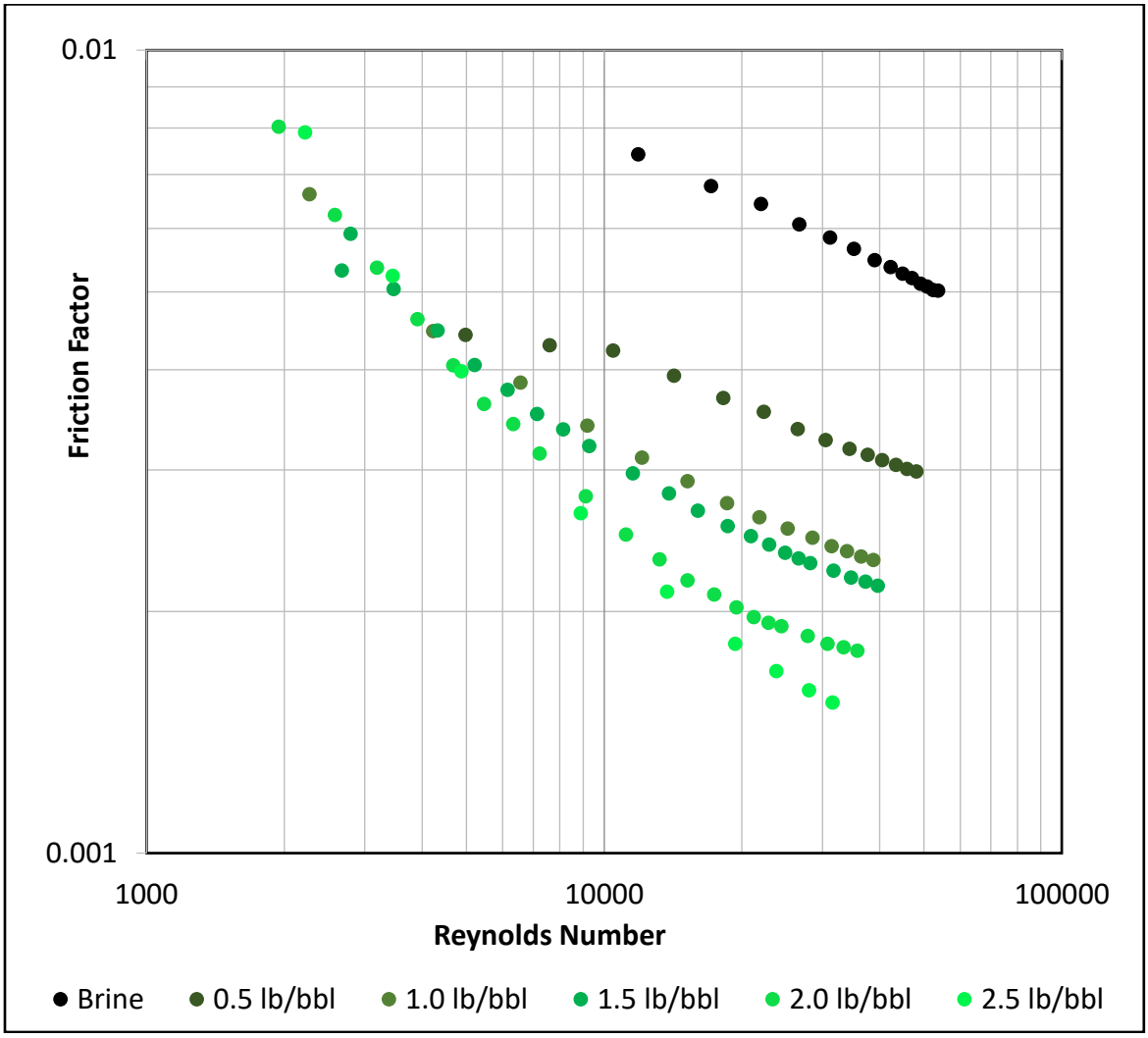

Figure 3.13: Experimental data from cesium formate brine in a 3/8 in OD tube at 150°F with xanthan concentrations from 0 to 2.5 lb/bbl.

At 230°F, the highest temperature tested in this study, the inversion in trends between the laminar and turbulent flow regimes occurred at even lower flow rates than in the 150°F test. Figure 3.14 shows pressure loss vs. flow rate for all polymer concentrations tested at 230°F in the ½ in OD tube. The pressure readings taken from different polymer concentrations at this temperature are closer together than those from the tests conducted at 100 and 150°F, suggesting that increasing fluid temperature reduces the effect that polymer concentration has on the magnitude of frictional pressure losses.

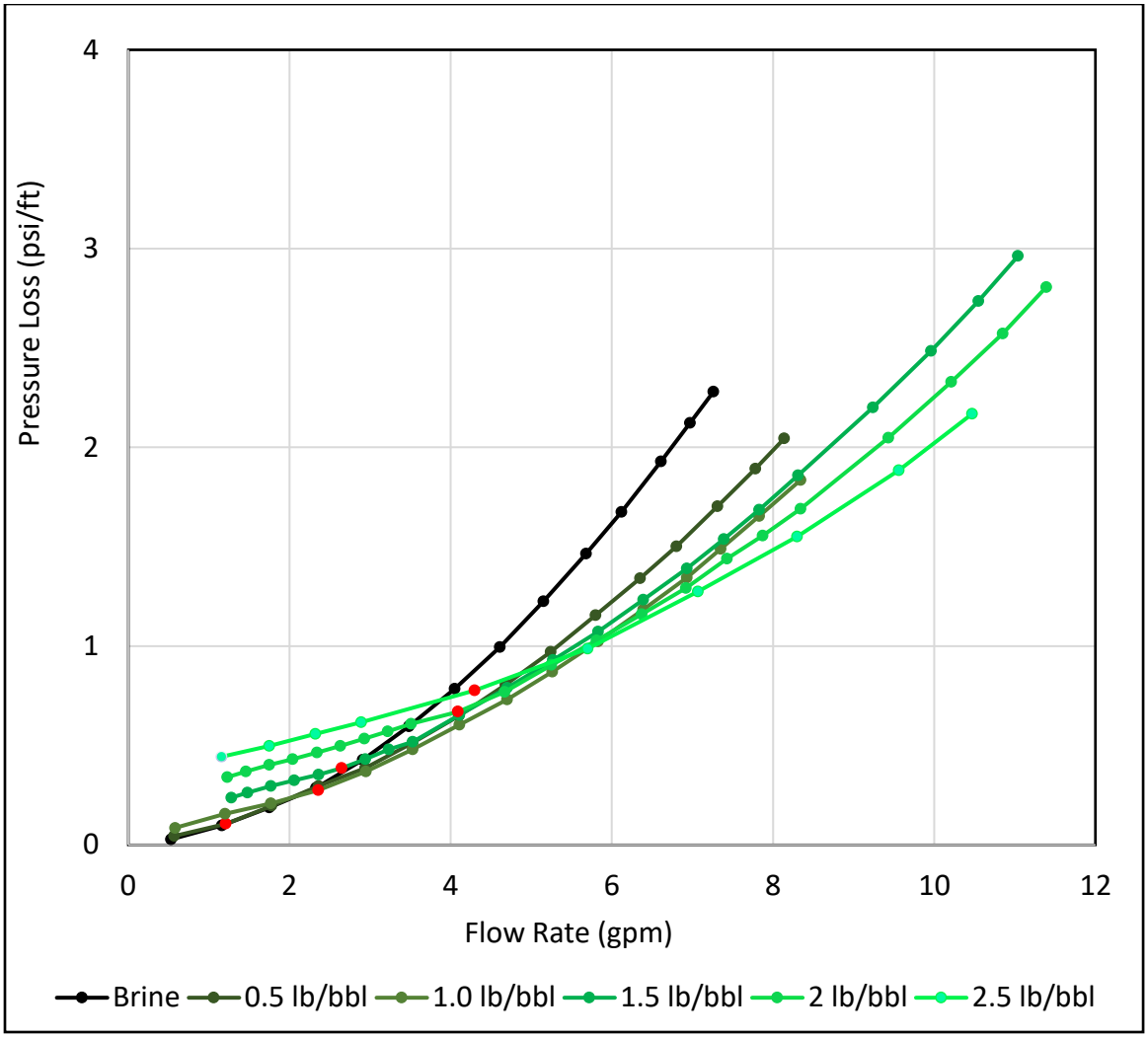

Figure 3.14: Experimental data from cesium formate brine in a ½" OD tube at 230°F with xanthan concentrations from 0 to 2.5 lb/bbl. Red dots represent the last laminar data point before the flow begins to transition to turbulence.

In aggregate, results from this study highlight the complexity of polymer additive behavior. Observed frictional pressure losses showed significant variation according to several factors including concentration, temperature, flow rate, and flow regime. Considering xanthan gum's common use as a thickening agent in drilling and completion

fluids, and the similarities in molecular structure between xanthan gum and many friction reducers, there appear to be commonalities in polymer additive behaviors regardless of the chemical's classification as a friction reducer or viscosifier.

3.3.3 Effect of Temperature on Frictional Pressure Loss

Data from fluids with identical polymer concentrations tested at differing temperatures were compared to gain insight into the effect of temperature on frictional pressure loss. As expected, experimental results showed a decrease in pressure losses with increasing temperatures in the laminar, transitional and turbulent flow regimes. However, the effect of temperature was observed to diminish beyond 150°F during experimentation with different polymer concentrations. Figure 3.15 shows pressure loss vs flow rate data collected from the ½ in OD test section at three different temperatures (100°F, 150°F and 230°F) in cesium formate brine with a polymer concentration of 2.0 lb/bbl.

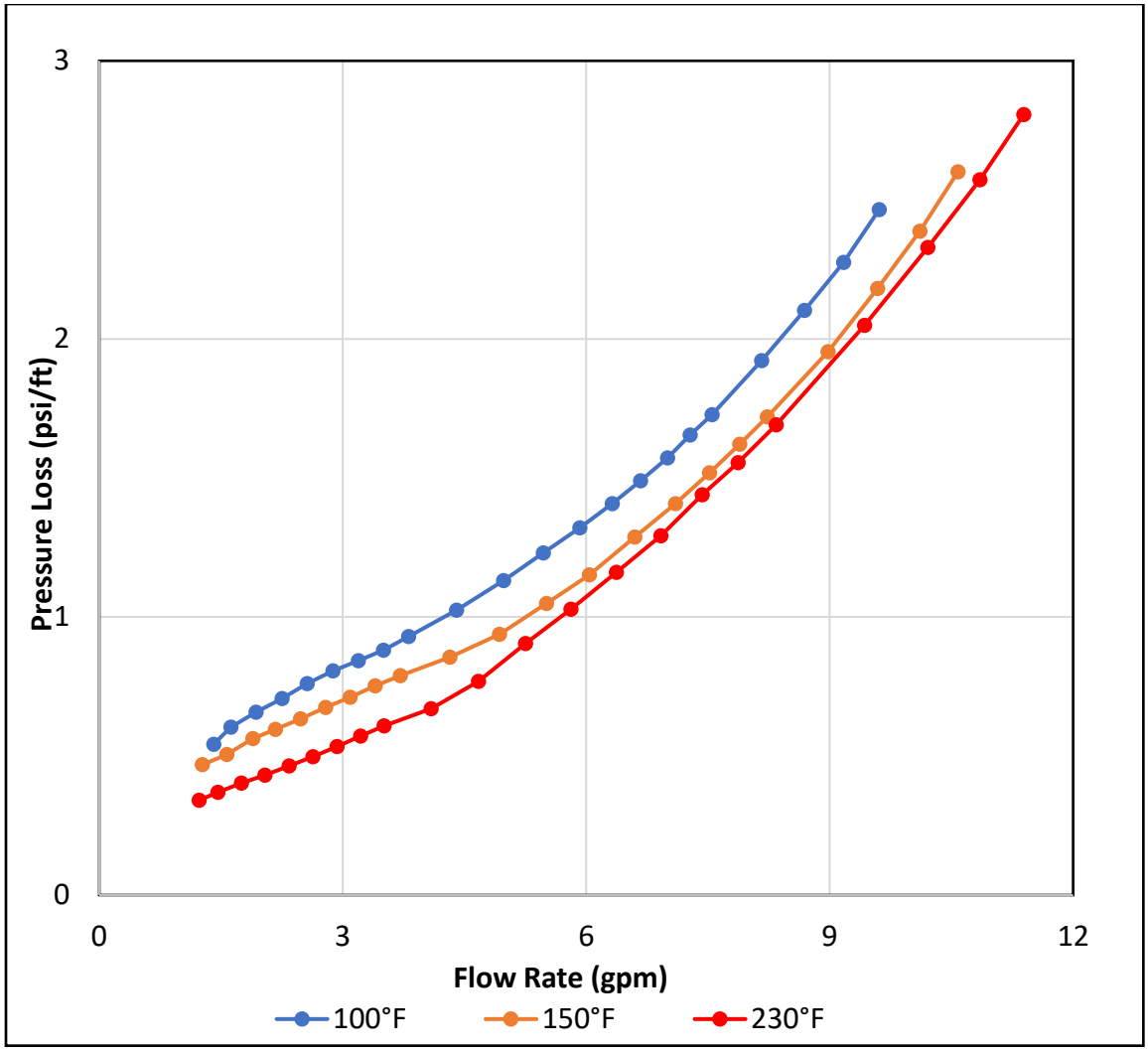

Figure 3.15: Frictional pressure loss in cesium formate brine containing 2.0 lb/bbl of xanthan gum at 100°F, 150°F and 230°F for the ½ in OD test pipe

Common industry practice for drilling mud rheology measurement involves testing at only one temperature, complicating any attempt to accurately model the complex behavior demonstrated here. These observations support the importance of real-time friction factor monitoring for more effective ECD management.

3.3.4 Effect of Shear Degradation on Frictional Pressure Loss

Experimental results thus far have proven that fluid composition and temperature have significant effects on frictional pressure loss and the accuracy of drilling hydraulics calculations. These are two of many factors that must be considered when performing high-fidelity hydraulic calculations. Variation of fluid characteristics over time is another important factor in this process.

To evaluate how the previously described polymer behavior is affected by time, frictional pressure loss was measured before and after fluids of identical polymer concentration experienced several hours of shearing within the experimental setup. Figure 3.16 shows pressure loss vs. flow rate data collected before and after a fluid containing 1.25 lb/bbl xanthan was sheared for approximately 10 hours. Reynolds numbers during these tests ranged from 220 to 8,320 for the un-sheared fluid and from 620 to 10,530 for the sheared fluid. In laminar flow the un-sheared fluid showed higher frictional pressure losses compared to the sheared fluid. In turbulent flow, however, the un-sheared fluid displayed decreased frictional pressure losses in comparison to the heavily sheared fluid.

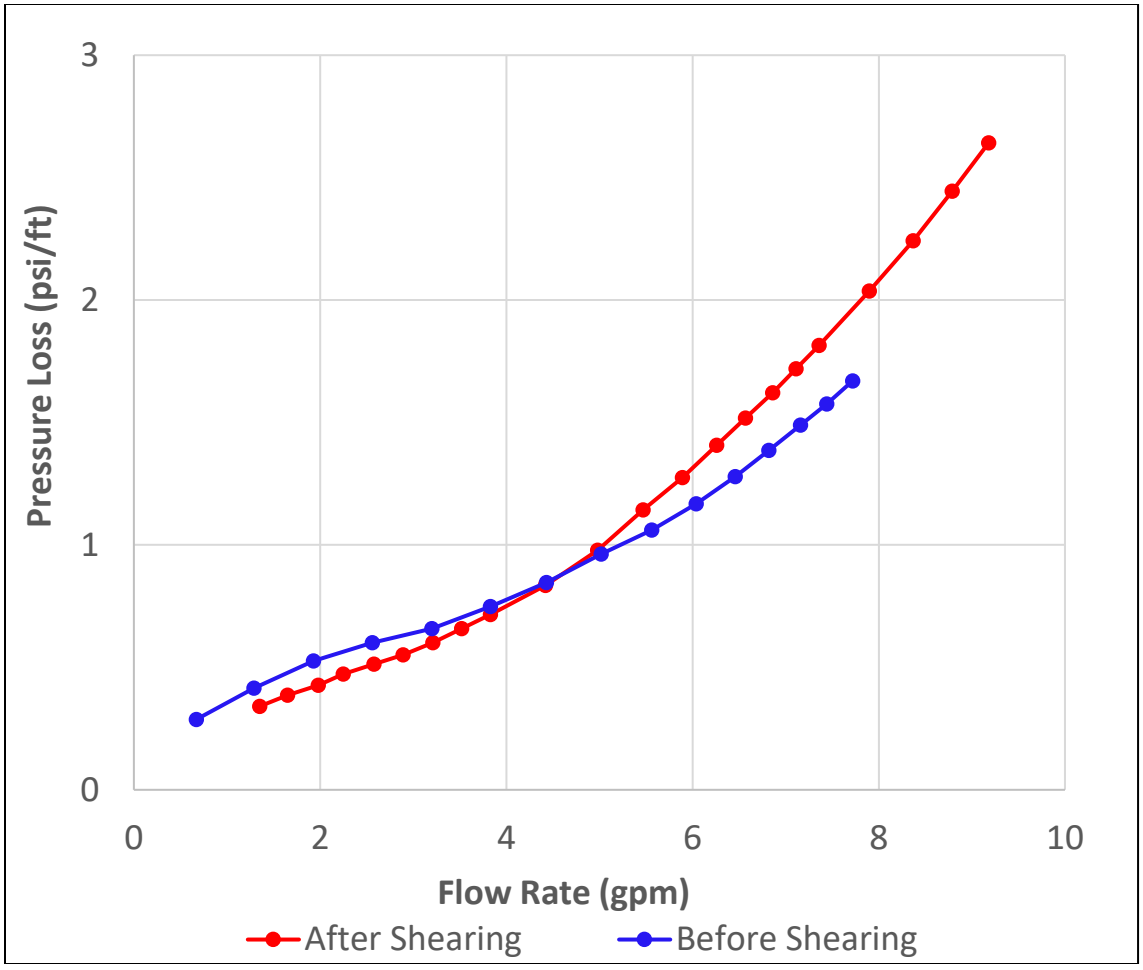

Figure 3.16: Frictional pressure loss in cesium formate brine containing 1.25 lb/bbl of xanthan gum at 100°F before and after shearing.

Interestingly enough, these two lines intersect and cross near the transition to turbulence the same way that data series from different polymer concentrations do in Figure 3.9 and Figure 3.11. The relationship between the two curves therefore resembles the trend between two fluids with slightly different polymer concentrations.

The tendency of long-chain polymer fluids to degrade at high shear rates has been extensively documented in literature (Fisher and Rodriguez, 1971; Tsau et al., 1992;

Karami et al., 2018). Polymer degradation due to shear degrades the polymer's effectiveness at reducing frictional pressure losses, complicating drilling hydraulics modeling. These complications are likely to produce erroneous prediction of frictional pressure drop and ECD accordingly, highlighting the importance of real-time automated measurements of friction factor for hydraulic planning and ECD management.

3.3.5 Demonstration of Data-Driven Prediction

As the data from this study demonstrate, existing methods for predicting frictional pressure losses are inadequate for modeling polymer drilling fluids in turbulent flow. The next step in this investigation is to evaluate a method for real time friction factor measurement in turbulent flow. This method is explained in further detail in Section 2.2.2.

To evaluate this method, data from a single test was filtered to include only turbulent data points and used to generate a graph of friction factor vs. Reynolds number, shown in Figure 3.17. A power law equation was then fitted to the data series. This equation was used to predict pressure readings for the same turbulent data points, allowing the accuracy of this prediction method to be evaluated. An R^2 value of 0.9896 was obtained for the curve fit, and a visual inspection of the trend line when compared to the experimental data shows that the fit correlates very well with the data series.

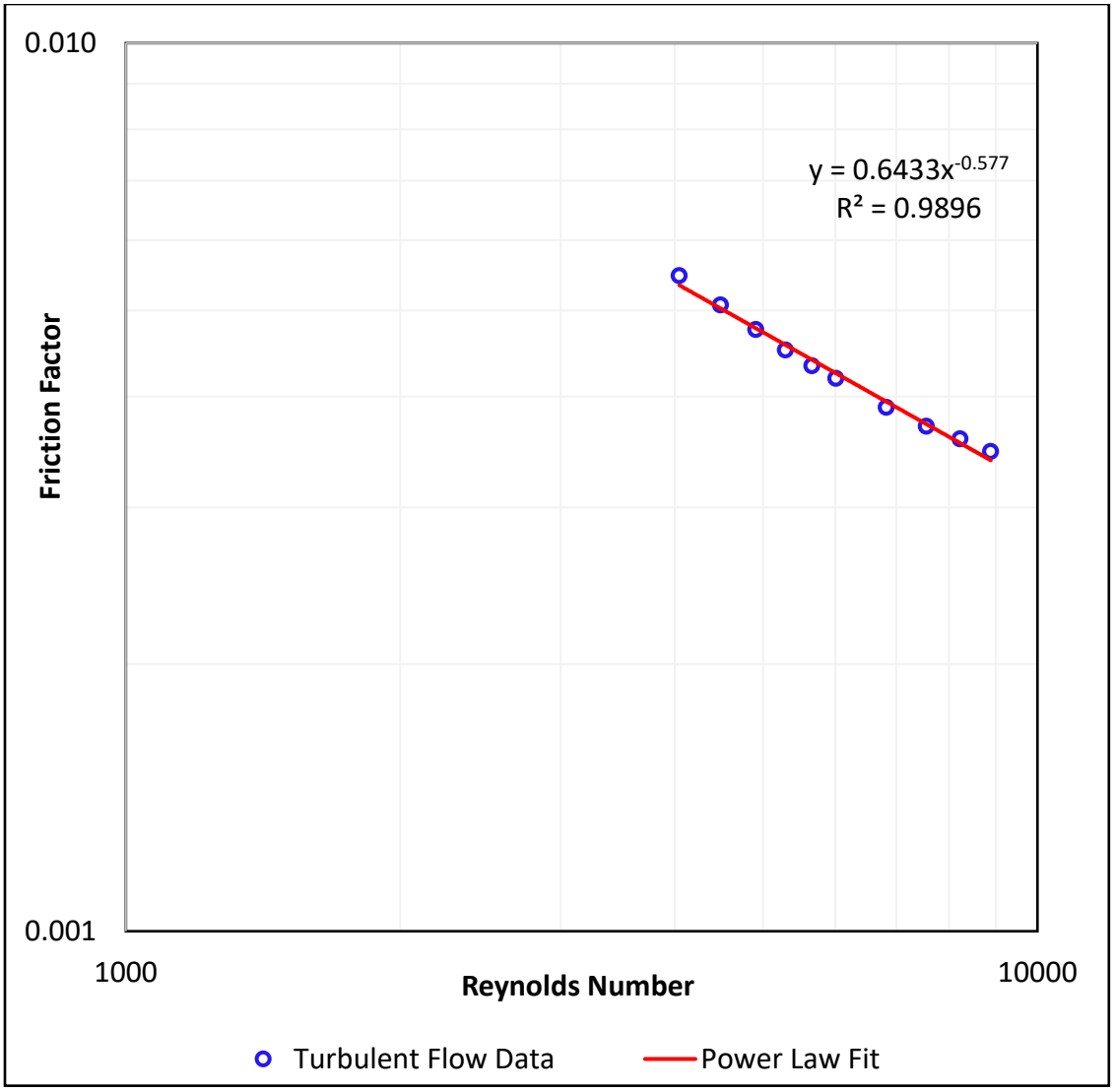

Figure 3.17: Friction factor vs. Reynolds number data for cesium formate brine containing 2.5 lb/bbl of xanthan gum tested at 100°F.

After the equation from this curve fit was used to "predict" the pressure readings for the entire test, experimental values were compared to the pressure readings simulated using this method. Figure 3.18 shows the results of this pressure prediction, with the previously evaluated model included for comparison.

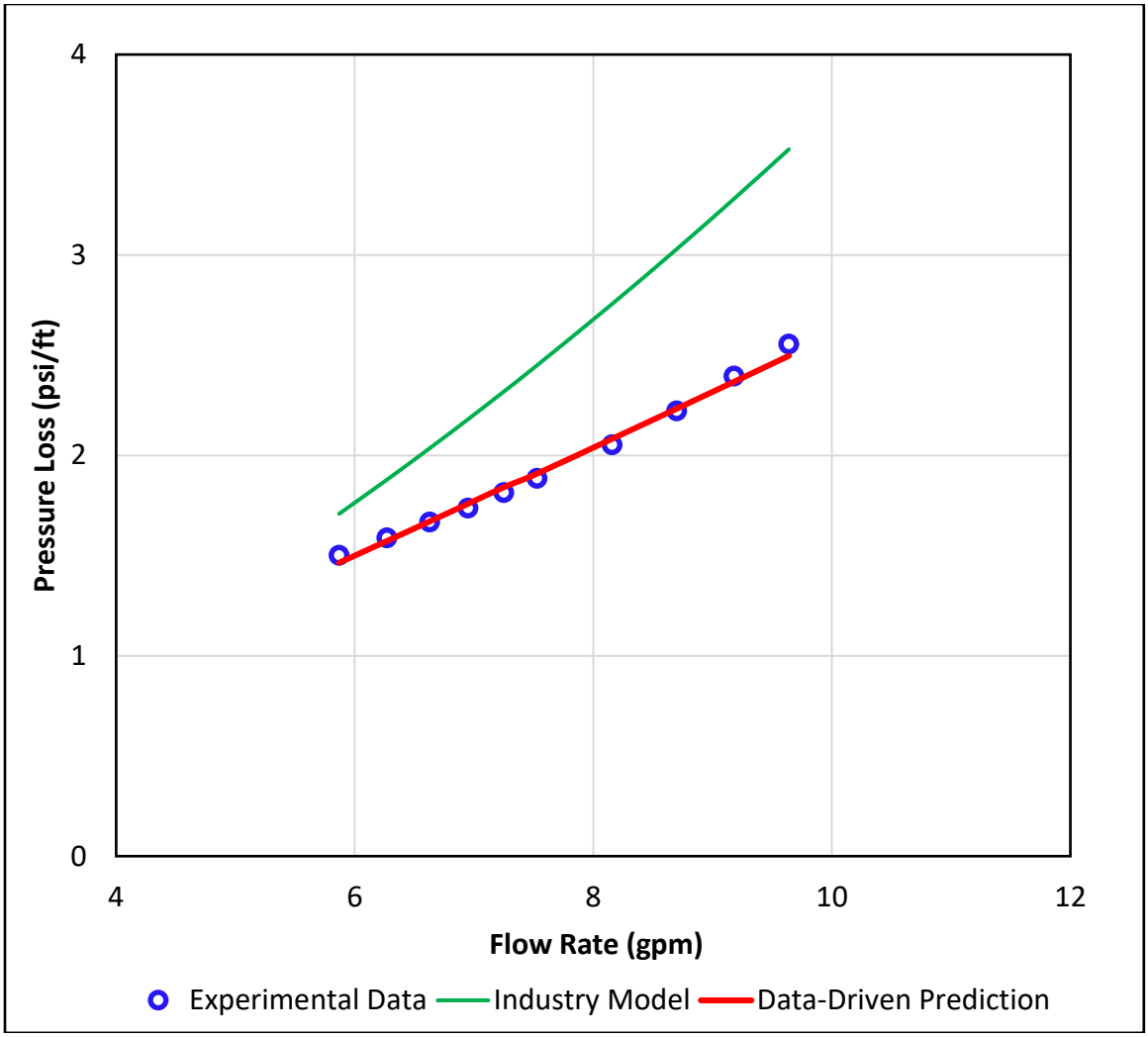

Figure 3.18: Results of real-time friction factor determination for a fluid containing 2.5 lb/bbl of xanthan at 100°F, compared to the previously evaluated industry standard method.

The real-time measurement method generated a maximum error of 2.0% for a single data point, compared to an error of 38.0% for the industry model. Average error values across the entire data series were 1.3% and 19.9% for the curve fit and industry prediction methods, respectively. Clearly, the real-time determination method provides substantially more accurate results than the established industry method.

3.4 Conclusions & Future Work

A comprehensive study of long-chain polymer additive behavior in drilling fluids yielded several important results. First, commonly used industry methods for modeling frictional pressure losses in turbulent flow of drilling fluids were shown to be inaccurate when there was substantial long-chain polymer content in the mud. This is likely because the polymers, valued for their thickening effect in laminar flow, take on the behavior of drag-reducing additives when the solution transitions to turbulence. The presence of these additives also delays the transition to turbulence, further complicating the process of modeling frictional pressure losses in all flow regimes.

Increasing fluid temperature caused a decrease in frictional pressure losses, but this effect was not linear. Heating the fluid from 100°F to 150°F had a greater impact on frictional pressure losses than further heating from 150°F to 230°F. Degradation of the fluid under high shear rates also had a significant effect on frictional pressure losses.

Real-time measurement of friction factors was shown to be a much more effective method for predicting frictional pressure losses than empirical correlations from literature. Pressure predictions could be significantly improved by a real-time measurement system on the rig, which can be used to characterize the fluids experimentally at the same time as they are used in the drilling process.

Data collected from testing a variety of muds onsite could be added to a database and used to improve the quality of predictive algorithms. Rather than attempting to build a

mathematical correlation that is valid for all potential drilling fluid makeups and flow conditions, historical data from similar fluids can be used to predict pressure loss value for the given scenario. Recent improvements in machine learning techniques, pattern recognition, and inexpensive computing power have made such an approach feasible. Future work in this area could show promising results.

Chapter 4

Automated Pipe Viscometer Development

The rotational viscometer, currently the industry standard for determining the rheological parameters of drilling fluid on the rig, has several shortcomings, as described in Section 2.1.2 . A new method of measuring rheological parameters has the potential to resolve these issues. This technology, called a pipe or capillary viscometer, has long been utilized for other applications such as food processing and enhanced oil recovery (Liauh and Liu, 1984; Suzuki, 1994). Maglione et al. (1996) applied the pipe viscometer concept to drilling fluids, demonstrating that standpipe pressure data could be used to determine the YPL parameters of a mud sample. Karimi Vajargah and van Oort (2015) developed the concept further, using downhole pressure data from wired drill pipe to perform rheology calculations, which provided more accurate rheological parameters at downhole conditions. Karimi Vajargah et al. (2016) applied the pipe viscometer concept to a laboratory flow loop, proving the technology's potential as a standalone measurement device. Ahmed and Miska (2009) state that pipe viscometers often provide more accurate rheological measurements than rotational viscometers.

A pipe viscometer requires the same equipment as the experimental setup described in Section 3.2: a pump, flow meter, a length of straight pipe, and sensors for measuring frictional pressure losses in laminar flow. The rheological parameters of the fluid can be determined by performing a relatively simple numerical analysis on this data. This system

is simpler to automate than a standard rotational viscometer, which tends to experience plugging issues when placed in-line in a mud sampling system. Pipe viscometers can also measure pressure losses in turbulent flow, providing drilling engineers with valuable additional information.

4.1 Background

Rheological parameters are determined in any viscometer system by fitting a curve to a graph of wall shear stress, τ_w, vs. shear rate, γ. These two parameters must therefore either be measured directly or calculated from other sensor readings. Sensors in a pipe viscometer system measure mass flow rate, density, temperature, and differential pressure across a length of straight pipe with a known inner diameter. The wall shear stress is calculated using Equation 4.1:

$$\tau_w = \frac{D}{4}\frac{dp}{dl} \tag{4.1}$$

where $\frac{dp}{dl}$ is the frictional pressure loss per unit length in laminar flow, determined by measuring the differential pressure between two points separated by a known distance.

Determination of γ from the data collected by a pipe viscometer system requires more calculation. For Newtonian fluids, calculating the shear rate is relatively simple. The nominal Newtonian shear rate is represented by Equation 4.2:

$$\gamma = \frac{8v}{D} \tag{4.2}$$

Where v is the average fluid velocity in the pipe, determined by Equation 4.3:

$$v = \frac{Q}{A} \tag{4.3}$$

Where Q is the volumetric flow rate and A is the internal cross-sectional area of the pipe from which differential pressure is measured.

Because most drilling fluids are non-Newtonian, a correction factor N must be applied to the nominal Newtonian shear rate to generate accurate data for a rheological curve fit. Equation 4.4 can be used to determine the shear rate at the wall for a non-Newtonian fluid (Ahmed and Miska, 2009):

$$\dot{\gamma}_w = \frac{3N+1}{4N}\frac{8v}{D} \tag{4.4}$$

Where N, known as the flow behavior index, is determined by:

$$N = \frac{d(\ln(\tau_w))}{d\left(\ln\left(\frac{8v}{D}\right)\right)}$$

The flow behavior index N for any given data point is therefore the slope of the curve $ln(\tau_w)$ vs. $\ln\frac{8v}{D}$ at that point. N values for all data points in a pipe viscometer test

can be found by fitting a second order polynomial function to the curve and then calculating the derivative for each point.

Once τ_w and $\dot{\gamma}_w$ have been calculated, a second curve fit can be performed to determine the YPL parameters as described in Section 2.1.2.

4.2 Laboratory Prototype

Sullivan (2016) used the previously described flow loop at The University of Texas at Austin to provide proof of concept for the pipe viscometer in the drilling fluids domain. Several fluids were tested, rheology calculations were performed on the data collected, and results were compared to measurements of the same fluid performed on an industry standard rotational viscometer. This study concluded that a pipe viscometer is capable of measuring the rheological parameters of a fluid to a high degree of accuracy when compared to a rotational viscometer system.

4.3 Initial Field Prototype

While the conclusions in Sullivan's (2016) study are promising, proving that a technology works in the laboratory does not necessary justify its widespread adoption in the field. In a large, capital-intensive business like the drilling industry, new techniques must be extensively tested before they are trusted to replace established standards. A prototype mud monitoring system donated from industry was adapted to function as a pipe viscometer to facilitate this field trial process. Although the donated system contained most

of the components necessary for a pipe viscometer, several modifications had to be made to collect, process and display data in the appropriate manner.

The prototype system is equipped with a pump, heater, Coriolis flow meter, rotational viscometer, oil/water cut analyzer, and two lengths of straight pipe with pressure sensors on each end. Its control and data acquisition system is exceedingly complex, featuring a top-of-the-line programmable logic controller (PLC) made by Allen Bradley. Data can be gathered from many remote sensors all over the rig using this system. Unfortunately, although all necessary sensors for a pipe viscometer system were present, the PLC did not have the software necessary to calculate rheological parameters from the data collected. Lack of customizability of the control and data processing software presented a significant obstacle to the adaptation of the system.

To avoid the excessive costs necessary to reprogram or retrofit the PLC, a Raspberry Pi mini-computer (shown in Figure 4.1) was connected to send external commands and collect data. The small size, low cost, and versatility of this component made it ideal for this application.

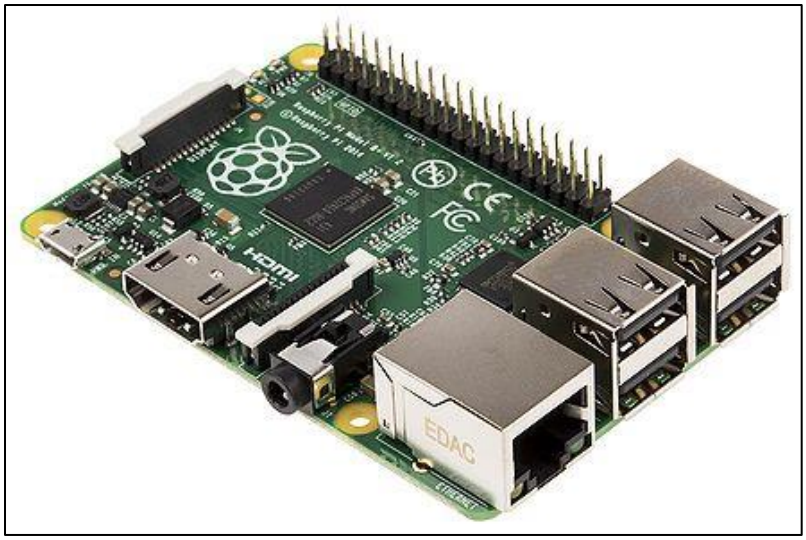

Figure 4.1: Raspbery Pi mini-computer (Prashar, 2016).

The Raspberry Pi connects to the Allen Bradley PLC via a CAT5 ethernet cable. Python code was written to send commands and retrieve data using a freely available Python library called Pycomm to interface with the PLC operating system. When testing the rheology of a fluid the Python script sends a series of commands to the PLC, directing the pump to step through a series of at least five flow rates. Each pump speed is held for at least 60 seconds to allow the flow inside the loop to reach steady state.

During this process, pressure readings are retrieved from the PLC and stored in a comma separated value (CSV) file on the Raspberry Pi. At the end of each test, the program retrieves the last 10 seconds of data from each flow rate, finds the median pressure value to eliminate outliers, and saves this value for input into the rheology curve fitting process described in Section 4.1. Data processing and graphing are performed with the assistance of Python libraries numpy and matplotlib. Another library called Tkinter generates the

graphical user interface (GUI), allowing the user to interact with the system and send commands.

4.4 Future Work

Initial field trials are the next step in the road to commercialization for pipe viscometer technology. A comprehensive study should be performed on the reliability and usefulness of the prototype, ideally over the course of drilling an entire well. Rotational viscometer data should be frequently collected and compared to that of the pipe viscometer to establish the feasibility of this new technology for replacing traditional methods. Real-time rheology data should be provided to the decision makers on the rig so that they can determine the value added to drilling operations. All test data should be archived with careful documentation so that it can be utilized for further study and drilling fluid characterization in the future.

Experiments should also be conducted to find the optimal dimensions for a pipe viscometer system, which will simplify the construction of future prototypes. Once a standard design has been developed and performance uncertainty has been minimized, several more prototypes can be constructed to test the long-term value of this technology. The feasibility of a helical pipe design should also be thoroughly analyzed during this process, potentially leading to the construction of a prototype.

Chapter 5

Conclusion

The experimental investigation presented in this work shows the substantial complications introduced into the drilling hydraulics modeling process by the presence of commonly used long-chain polymer additives. Despite decades of research attempting to create a comprehensive methodology for predicting pressure losses in non-Newtonian fluids, the best methods in use today still fall short under certain conditions.

An alternative offered by real-time measurement method for determining frictional pressure losses in drilling operations was proposed and evaluated, showing promising results. With a flow loop system located on the rig site for measuring friction factor in real time, the complications associated with modeling turbulent flow of drilling fluids can be avoided altogether. Data generated by such a system can be collected and eventually used to predict downhole pressure losses without the need for an onsite system.

Furthermore, the same equipment required to measure frictional pressure losses in real time can also be used to determine the rheological parameters of the fluid using the pipe viscometer concept. This idea has been proven in the lab, and substantial progress has been made towards the production of a functioning field prototype. Field trials of this technology will evaluate the effectiveness of such a system and the utility of the real-time rheology data it provides.

By integrating the various novel techniques described in this work, a business case can be made for the widespread adoption and use of real-time fluid measurement techniques in drilling operations. Beyond the previously described benefits of such a system, the vast amounts of data generated by deployment of these systems could open an entirely new field in the study of fluid mechanics. Machine learning techniques can be applied to the data from these systems to generate new algorithms for predicting fluid behavior, allowing for many more independent variables to be accounted for than would otherwise be possible.

References

Ahmed, R., and Miska, S.Z. Advanced wellbore hydraulics, Chapter 4.1, (pp. 191-219). Advanced drilling and well technology. USA Society of Petroleum Engineers. Ed. Bernt S. Aadnoy. SPE, 2009.

American Petroleum Institute, 2010. Recommended Practice 13D, Rheology and Hydraulics of Oil-well Fluids.

Bailey, W.J., Peden, J.M., 2000. A generalized and consistent pressure drop and flow regime transition model for drilling hydraulics. SPE Drilling & Completion, 15.

Beck, F.E., Powel, J.W., Zamora, M.: "A Clarified Xanthan Drill-in Fluid for Prudhoe Bay Horizontal Wells," SPE 25767, SPE/IADC Drilling Conference, Amsterdam, The Netherlands, Feb 23-25, 1993

Bommer, P. (2015a). *Introduction to Drilling Engineering: Example Well.* [PowerPoint slides]. Retrieved from https://canvas.utexas.edu/

Bommer, P. (2015b). *Introduction to Drilling Engineering: Introduction to Drilling Mud.* [PowerPoint slides]. Retrieved from https://canvas.utexas.edu/

Cholet, H. 1997. Progressing Cavity Pumps. Paris, France: Inst. Francais du Petrole.

Collins, M., & Schowalter, W. R. (1963). Behavior of non-Newtonian fluids in the entry region of a pipe. AIChE journal, 9(6), 804-809.

Continental Ultra Pumps. (2016). 2CL6 Progressing Cavity Pump [Digital image]. Retrieved from http://www.continentalultrapumps.com/store/cl6-progressing-cavity-pumps-new.html

Dodge, D.W. and Metzner, A.B. 1959. Turbulent Flow of Non-Newtonian Systems. AIChE J. 5 (2): 189–204.

Dosunmu, Idowu T., and Subhash N. Shah. "Evaluation of friction factor correlations and equivalent diameter definitions for pipe and annular flow of non-Newtonian fluids." Journal of Petroleum Science and Engineering 109 (2013): 80-86.

Fischer, C.C. Navarrete, Constien, V.G., Coffey, Aasadi, M.: “Novel Application of Synergistic Guar/NonAcetylated Xanthan Gum Mixtures in Hydraulic Fracturing,” paper SPE 65037 presented at the 2001 SPE International Symposium on Oilfield Chemistry, Houston, Texas, Feb. 13-16.

Fisher, D. H. and Rodriguez, F. (1971), Degradation of drag-reducing polymers. J. Appl. Polym. Sci., 15: 2975–2985. doi:10.1002 / app.1971.070151207

García-Ochoa, F., Santos, V. E., Casas, J. A., & Gómez, E. (2000). Xanthan gum: Production, recovery, and properties. England: Elsevier Inc. doi:10.1016/S0734-9750(00)00050-1

Gardco. (2017). byko-visc Basic [Digital image]. Retrieved from https://www.gardco.com/pages/viscosity/vi/rotational_viscometers.cfm

Graham, M. D. (2004). Drag reduction in turbulent flow of polymer solutions. Rheology reviews, 2(2), 143-170.

Hemphil, T., Campos, W., Tehrani, M.A., 1993. Yield power-law model mode accurately predicts mud rheology. Oil Gas J. 91, 45.

Herschel, W.H., Bulkley, R., 1926. Konsistenzmessungen von Gummi-Benzollosungen. Kolloid Z. 39, 291.

Hoyt, J. W. (1972, June). The Effect of Additives on Fluid Friction. Transcation of the ASME: Journal of Basic Engineering, 94(2), 258-285.

Hoyt, J. W., & Fabula, A. G. (1964). The Effect of Additives on Fluid Friction. Fifth Symposium on Naval Hydrodynamics, Ship Motions, and Drag Reduction, (pp. 947-974). Bergen, Norway.

Karami, H.R., Rahimi, M. & Ovaysi, S. Korean J. Chem. Eng. (2018) 35: 34. https://doi-org.ezproxy.lib.utexas.edu/10.1007/s11814-017-0264-1

Karimi Vajargah, A., Sullivan, G., & van Oort, E. (2016, September 14). Automated Fluid Rheology and ECD Management. Society of Petroleum Engineers.

Karimi Vajargah, A., & van Oort, E. (2015, March 17). Automated Drilling Fluid Rheology Characterization with Downhole Pressure Sensor Data. Society of Petroleum Engineers. doi:10.2118/173085-MS

Kelessidis, V.C., Dalamarinis, P., Maglione, R. Experimental study and predictions of pressure losses of fluids modeled as Herschel–Bulkley in concentric and eccentric annuli in laminar, transitional and turbulent flows, Journal of Petroleum Science and Engineering, Volume 77, Issues 3–4, June 2011, Pages 305-312.

Kelessidis, V.C., Christidis, G., Makri, P., Hadjistamou, C., Tsamantaki, C., Mihalakis, A., Papanicolaou, C., Foscolos, A., 2007. Gelation of water–bentonite suspensions at high temperatures and rheological control with lignite addition. Appl. Clay Sci. 36, 221.

Khan, R., Kuru, E., Trembla, B., & Saasen, A. (2003, January 1). An Investigation of Formation Damage Characteristics of Xanthan Gum Solutions Used for Drilling, Drill-In, Spacer Fluids, and Coiled Tubing Applications. Petroleum Society of Canada. doi:10.2118/2003-067

H., Li, W.D. and Tian, J. Liu, Y.Z.: "Pilot Test of Xanthan Gum Flooding in Shengli Oilfield," paper SPE 57294, SPE Asia Pacific Improved Oil recovery Conference, Kuala Lumpur, Malaysia, Oct. 25-26, 1999.

Maglione, R., Gallino, G., Robotti, G., Romagnoli, R., & Rommetveit, R. (1996, January 1). A Drilling Well as Viscometer: Studying the Effects of Well Pressure and Temperature on the Rheology of the Drilling Fluids. Society of Petroleum Engineers. doi:10.2118/36885-MS

Mehrabi, M., Zeyghami, M., & Shahri, M. P. (2012, January 1). Modeling of Fracture Ballooning in Naturally Fractured Reservoirs: A Sensitivity Analysis. Society of Petroleum Engineers. doi:10.2118/163034-MS

Munson, B. R., 1940, Okiishi, T. H. 1939- (Theodore Hisao), Huebsch, W. W., & Rothmayer, A. P., 1959. (2013). Fundamentals of fluid mechanics (7th ed.). Hoboken, NJ: John Wiley & Sons, Inc.

Navarrete, R. C., Dearing, H. L., Constien, V. G., Marsaglia, K. M., Seheult, J. M., & Rodgers, P. E. (2000, January 1). Experiments in Fluid Loss and Formation Damage with Xanthan-Based Fluids While Drilling. Society of Petroleum Engineers. doi:10.2118/62732-MS

PetroWiki. (2018). Positive displacement pumps. http://petrowiki.org/Positive_displacement_pumps?rel=1 (accessed 5 January 2018)

Prashar, A. (25 August 2016). Raspberry Pi 2 [Digital image]. Retrieved from https://insights.ubuntu.com/2016/08/25/25-linux-devices-to-celebrate-25-years-of-linux

Schulz, D. N., 1943, Glass, J. E. 1937- (J. Edward), & American Chemical Society. Division of Polymeric Materials: Science and Engineering. (1991). Polymers as rheology modifiers. Washington, D.C: American Chemical Society.

Salamone, J.C., Clough, S.B., Salamone, A. Beal, Reid, K.I.G., Jamison, D.E.: "Xanthan Gum- A Lyotropic Crystalline Polymer and its Properties as a Suspending Agent," SPE 9097 SPEJ Forum Article,1982.

Slashme. (24 May, 2015). Rheology of time independent fluids [Digital image]. Retrieved from https://commons.wikimedia.org/wiki/File:Rheology_of_time_independent_fluids.svg

Sullivan, G. (2016). *Automated Characterization of Drilling Fluid Properties* (Master's thesis). Retrieved from https://repositories.lib.utexas.edu/handle/2152/46772

Subramanian, R., & Azar, J. J. (2000, January 1). Experimental Study on Friction Pressure Drop for non-Newtonian Drilling Fluids in Pipe and Annular Flow. Society of Petroleum Engineers. doi:10.2118/64647-MS

Toms, B. A. (1948). Some Observations on the Flow of Linear Polymer Solutions through Straight Tubes at Large Reynolds Numbers. Proceedings of the 1st International Congress on Rheology, 2, 135-141.

Tsau, J. S., Liang, J. T., Hill, A. D., & Sepehrnoori, K. (1992, February 1). Re-Formation of Xanthan/Chromium Gels After Shear Degradation. Society of Petroleum Engineers. doi:10.2118/18506-PA

Virk, P. S. (1975). Drag reduction fundamentals. AIChE Journal, 21(4), 625-656. doi:10.1002/aic.690210402

Zamora, M., Roy, S., Slatter, K., 2005. Comparing a basic set of drilling fluid pressure-loss relationships to flow-loop and field data. Paper AADE-05-NTCE-27. Proceedings of AADE National Technical Conference and Exhibition, Houston (USA).